



저작자표시-비영리-변경금지 2.0 대한민국

이용자는 아래의 조건을 따르는 경우에 한하여 자유롭게

- 이 저작물을 복제, 배포, 전송, 전시, 공연 및 방송할 수 있습니다.

다음과 같은 조건을 따라야 합니다:



저작자표시. 귀하는 원저작자를 표시하여야 합니다.



비영리. 귀하는 이 저작물을 영리 목적으로 이용할 수 없습니다.



변경금지. 귀하는 이 저작물을 개작, 변형 또는 가공할 수 없습니다.

- 귀하는, 이 저작물의 재이용이나 배포의 경우, 이 저작물에 적용된 이용허락조건을 명확하게 나타내어야 합니다.
- 저작권자로부터 별도의 허가를 받으면 이러한 조건들은 적용되지 않습니다.

저작권법에 따른 이용자의 권리는 위의 내용에 의하여 영향을 받지 않습니다.

이것은 [이용허락규약\(Legal Code\)](#)을 이해하기 쉽게 요약한 것입니다.

[Disclaimer](#)

Ph.D. Dissertation of Biomedical Sciences

Phase separation–mediated
control of nArgBP2 underlies the
structural plasticity of dendritic
spines

nArgBP2의 액상 간 상분리 현상을 통한
구조적 가소성 조절 기전에 관한 연구

August 2023

The Department of Biomedical Sciences
Seoul National University College of Medicine

Eunji Cho

nArgBP2의 액상 간 상분리 현상을
통한 구조적 가소성
조절 기전에 관한 연구

지도교수 장 성 호

이 논문을 의학박사 학위논문으로 제출함
2023년 4월

서울대학교 대학원
의과학과 신경과학/생리학 전공
조 은 지

조은지의 박사 학위논문을 인준함
2023년 7월

위 원 장

부위원장

위 원

위 원

위 원

Abstract

Ablation of nArgBP2, a candidate gene of intellectual disability (ID), caused defects in spine maturation and excitatory synapse formation in developing neurons. Interestingly, I found that the KD of nArgBP2 in mature neurons did not lead to any observable morphological abnormalities in the preexisting spines during resting conditions, thereby prompting further inquiries into its functional role in mature neurons. However, I found that nArgBP2 KD completely abolished the enlargement of dendritic spines during chemically induced long-term potentiation (cLTP) in mature neurons.

I found that nArgBP2 forms biomolecular condensates in dendritic spines by phase separation and that these condensates are dispersed by cLTP. Liquid-liquid phase separation refers to the phenomenon where biomolecules, such as proteins and nucleic acids, undergo phase separation and form liquid-like droplets within cells. This process has emerged as a critical mechanism for regulating various biological processes, including cellular organization, signal transduction, and gene expression.

nArgBP2 undergoes liquid-liquid phase separation through multivalent intermolecular interactions mediated by SH3 domains and proline-rich domains. Furthermore, nArgBP2 forms coacervates with CaMKII α , which undergoes rapid disassembly upon calcium/CaMKII α -dependent phosphorylation. I further showed that the interaction between nArgBP2 and WAVE1 counteracts condensate formation.

Together, these findings strongly suggest that in the resting state, nArgBP2 is sequestered within condensates, but it is released due to CaMKII α -mediated phosphorylation during synaptic plasticity. Subsequently, the released nArgBP2 can engage in a timely interaction with WAVE1, thereby inducing spine head enlargement in mature neurons.

Also, there is a zinc finger motif in the NSE (Neural Specific Exon) domain of nArgBP2 and the role of the NSE domain has not been studied. I found that nArgBP2 mutant without NSE shows different localization of nArgBP2. Also, treatment with a high concentration of zinc ion makes nArgBP2 less prominent at dendritic spines. In addition to revealing the underlying mechanism of nArgBP2 functionality in mature neurons with zinc, these results also suggest its defect may contribute to the pathogenesis of neurological disorders.

This work is published in Exp Mol Med (2023).

Keyword : Phase-phase separation, nArgBP2, dendritic spine, structural plasticity

Student Number : 2016-23695

CONTENTS

Abstract	1
Contents	3
List of Figures and Tables	4
List of Abbreviations	6

Phase separation–mediated control of nArgBP2 underlies the structural plasticity of dendritic spines

Introduction.....	7
Material and Methods	11
Results	19
Discussion.....	59
Reference.....	67
Abstract in Korean	75

List of Figures and Tables

Figure 1. nArgBP2 KD in mature neurons does not result in morphological defects in existing dendritic spines.	32
Figure 2. Sustained expression of nArgBP2 during neuronal development, and confirmation of knock-down efficiency by nArgBP2 shRNA.....	33
Figure 3. nArgBP2 KD in mature neurons completely inhibits spine head enlargement during cLTP	34
Figure 4. Expression levels of NMDA receptors, GluN1 and GluN2 were not altered with nArgBP2 KD in hippocampal neurons.	35
Figure 5. 3D geometry analysis of dendritic spines during cLTP.	36
Figure 6. Expression of nArgBP2- <i>res</i> in ArgBP2 KD neurons showed similar expression levels to endogenous nArgBP2 levels	37
Figure 7. nArgBP2 forms condensates in the dendritic spines and these condensates are dispersed during chemical-LTP, which spatiotemporally coincides with spine head enlargement.....	38
Figure 8. Conservation of putative CaMKII phosphorylation sites across species, and the schematic figure of CaMKII phosphorylation-deficient mutant (3S3A).....	39
Figure 9. nArgBP2 forms condensates in the dendritic spines and these condensates are dispersed by CaMKII α -mediated phosphorylation.....	40
Figure 10 nArgBP2 ₉₅₉₋₁₁₉₆ droplets in living hippocampal neurons	41
Figure 11. nArgBP2 droplets are dissolved by 1,6-hexanediol in living hippocampal neurons	42
Figure 12. Endogenous nArgBP2 also formed liquid-like	

condensates in spines that were dispersed by 1,6-hexanediol treatment.	43
Figure 13. Biomolecular condensate assembly of nArgBP2 in heterologous systems with multivalent intermolecular interactions between SH3 domains and proline-rich domains	44
Figure 14. Biomolecular droplets of nArgBP2 <i>in vitro</i> and heterologous systems.....	45
Figure 15. nArgBP2 condensates in heterologous and <i>in vitro</i> expression systems shows liquid-like properties.	46
Figure 16. Biomolecular condensate co-assembly of nArgBP2 with CaMKII α and rapid dispersion by Ca ²⁺ /CaMKII α -mediated phosphorylation.....	48
Figure 17. WAVE1 binds to nArgBP2 and their interaction interferes with the phase-separating property of nArgBP2.....	50
Figure 18. Spine enlargement caused by nArgBP2 during cLTP is mediated by WAVE1 interaction.....	52
Figure 19. Model for the role of nArgBP2 in enlargement of dendritic spines during LTP	54
Figure 20. nArgBP2 ₉₅₉₋₁₁₉₆ also formed droplets in developing neurons but these droplets are reluctant to be dissolved by 1,6 hexanediol treatment.	55
Figure 21. The NSE domain of nArgBP2 is required for the efficient targeting of nArgBP2 to dendritic spines	56
Figure 22. nArgBP2 localization at dendritic spine is zinc dependent.	57
Figure 23. The schematic figure of role of nArgBP2.....	58

List of Abbreviations

ID: intellectual disability

BD: bipolar disorder

cLTP: chemical long-term potentiation

DIV: Days *in vitro*

FRAP: fluorescence recovery after photobleaching

KD: knockdown

nArgBP2: Neural Arg/c-Abl kinase binding protein 2

SORBS2: sorbin and SH3 domain-containing 2

SIM: structured illumination microscopy

shRNA: small hairpin RNA

WAVE: WASP-family verprolin-homologous protein

WASP: Wiskott-Aldrich syndrome protein

CaMKII α : Calcium/calmodulin-dependent protein kinase II α

INTRODUCTION

Dendritic spines are tiny protrusions arising from dendrites, in which most excitatory synapses are located¹. They act as chemically and electrically isolated micro-compartments participating in the formation of synapses and neuronal circuits. Activity-dependent maintenance or elimination of dendritic spines is critical for remodeling neural circuits during development, and synaptic plasticity². Dendritic spines are enriched for highly branched F-actin, and continuously change their morphology due to actin-regulating proteins localized to postsynaptic densities (PSDs). Therefore, the activity of the actin-regulating proteins has a major influence on the regulation of spine morphology and their abnormalities are closely related to various psychiatric disorders.

The neural Arg/c-Abl kinase binding protein 2 (ArgBP2/nArgBP2), alternatively referred to as sorbin and SH3 domain-containing 2 (SORBS2), is positioned within the chromosomal locus 4q35.1 in humans. This gene locus has been implicated in the etiology of ID disorders³. ArgBP2/nArgBP2 belongs to an adaptor protein family that includes vinexin and CAP/ponsin which are thought to participate in the regulation of cell adhesion, actin cytoskeleton organization, and growth factor receptor signaling⁴. This family is characterized by a sorbin homology (SoHo) domain in the NH₂-terminal region and three SH3 domains in the COOH-terminal region⁴⁻⁶. The neuron-specific nArgBP2 was found to localize to synapses interacting with the synapse-associated protein 90/Postsynaptic density (PSD)-95-associated protein (SAPAP)^{4,7}.

The SH3 domains of nArgBP2 bind to synaptojanin 1/2, dynamin 1/2, and Wiskott–Aldrich syndrome protein–family verprolin homologous protein (WAVE) 1/2. Down–regulation of nArgBP2/ArgBP2 expression in astrocytes induces the redistribution of focal adhesion proteins and an increase of peripheral actin ruffles⁷, suggesting that nArgBP2/ArgBP2 functions as an adaptor protein coordinating multiple signals regulating the balance between adhesion and motility of the actin cytoskeleton^{7,8}.

nArgBP2 knock–out (KO) mice have been reported to display manic/bipolar–like behavior resembling many aspects of the symptoms of patients with bipolar disorder (BD)⁹. In addition, copy number variation of nArgBP2 has been linked to ID¹⁰, and deletion of nArgBP2 led to impaired dendritic complexity and decreased frequency of amino–3–hydroxy–5–methyl–4–isoxazolepropionic acid receptor (AMPA) miniature spontaneous excitatory postsynaptic currents (EPSCs) in dentate gyrus granule cells, accompanied by ID–like behavioral deficits¹¹. Previously, our lab showed that the knockdown (KD) of nArgBP2 in developing neurons induces a profound alteration in dendritic spine morphology and leads to a specific impairment in the formation of excitatory spine–synapses. This disruption results in an imbalance between excitatory and inhibitory synaptic inputs (E/I imbalance)¹², which we proposed that it may underlie the causal mechanisms of ID. Recent studies have shown that abnormal functioning of postsynaptic SAPAP and SH3 and multiple ankyrin repeat domains protein (SHANK) proteins are closely related to the E/I imbalance, which accounts for various psychiatric disorders^{9,13,14}. Interestingly, these proteins interact with each other as well as with nArgBP2,

sharing many binding partners at synapses, suggesting that they may be responsible for the comorbidity seen in various psychiatric disorders¹⁵.

Besides its high expression in developing neurons, the sustained expression of nArgBP2 at high levels during maturation stages strongly suggests its functional significance in mature neurons, but despite having such profound effects on developing neurons, I found that nArgBP2 KD in mature neurons did not result in any morphological defects in existing dendritic spines at rest. I hypothesized that in resting mature neurons nArgBP2 exists in an “inactive” state, but is converted to the “active” state in response to Ca^{2+} influx during cLTP, which subsequently initiates downstream signal transduction leading to structural plasticity. As the underlying mechanism, I noted the phenomenon of liquid–liquid phase separation (LLPS) that has emerged as a fundamental mechanism for regulating various biological processes^{16,17}. LLPS is known to be triggered by multivalent interactions of intrinsically disordered regions or protein–interacting domains^{18,19}. Although whether LLPS plays a physiological role in living cells remains questionable^{16,17}, it is an attractive mechanism that may be involved in the spatiotemporal regulation of biological processes.

Through a series of experiments using living neurons, heterologous and *in vitro* expression systems, I demonstrated that nArgBP2 at rest is sequestered in the liquid condensates and is being released upon the CaMKII α –mediated phosphorylation during LTP, which regulates its interaction with WAVE1 to induce the enlargement of dendritic spines. Together, these findings can provide valuable

mechanistic insights into the role of nArgBP2 in the spatiotemporal regulation of dendritic spine structural plasticity. Moreover, these results suggest the possibility that abnormalities in the phase-separation dynamics of nArgBP2 could potentially underlie the observed synaptic dysfunction associated with intellectual disability (ID).

nArgBP2 is characterized by the presence of a neuronal-specific exon that is absent in ArgBP2. Despite this difference in nArgBP2 domain, the role of the NSE domain has not been studied. To investigate the function of NSE in nArgBP2, I used nArgBP2 mutant which has no NSE. GFP-nArgBP2 Δ NSE mutant was less prominent at spines, suggesting that NSE is required for nArgBP2 localization. Also, there is a zinc finger motif in the NSE domain of nArgBP2. Zinc-binding proteins require zinc for their structures and functions. Homeostasis of protein-bound and free zinc is critical to normal brain function. Most recently, it has been shown that adult neurogenesis in the brain depends on zinc and hippocampal functions including learning, memory, and regulation of emotion and mood. Thus, I suggest the possibility of NSE of nArgBP2 regulating zinc-dependent plasticity or interaction with other synaptic proteins, which certainly is of interest for further study.

MATERIALS AND METHODS

Materials and Methods

Animal experiments were approved by the Institute of Animal Care and Use Committee (IACUC, Approval ID number: SNU-100930-5) of Seoul National University, Korea. All experiments were carried out in accordance with approved guidelines and regulations.

DNA constructs and antibodies

RNA interference -mediated nArgBP2 knockdown was carried out by expressing small hairpin RNA (shRNA) duplexes in pSiren-U6-mRFP vector (Clontech, Palo Alto, CA) as previously described¹². Silent mutations within the shRNA targeting sequence (C593T, G596A, and A599G) in EGFP-nArgBP2 (EGFP-nArgBP2-*res*) were generated as previously described¹². EGFP-nArgBP2₉₅₉₋₁₁₉₆-3S3A and 3S3D were constructed using EZchange™ MultiSite-directed Mutagenesis kit (Enzynomics, Daejeon, South Korea). CaMKII α -SBFP2 was constructed by subcloning CaMKII α from CaMKII α -Venus (Addgene) by PCR in SBFP2-N1 vector. EGFP-mito-nArgBP2₉₅₉₋₁₁₁₀-2P2A was derived from EGFP-mito-nArgBP2₉₅₉₋₁₁₁₀ by introducing P1027A and P1030A mutations. CRY2 PHR (Addgene, Watertown, MA) was PCR-amplified and subcloned between the NotI and SalI sites of mCherry C1 vector, and nArgBP2₉₅₉₋₁₁₉₆ was subsequently subcloned upstream of the mCherry cDNA using SpeI and KpnI to construct nArgBP2₉₅₉₋₁₁₉₆-mCh-CRY2. EGFP-WAVE1 was constructed by subcloning the WAVE1 sequence into a pEGFP-C1 vector using BglII and EcoRI.

CaMKII α -SBFP2 was manipulated by amplifying the CaMKII α sequence from CaMKII α -Venus (Addgene) by PCR and subcloning it between the XhoI and BamHI sites of SBFP2 N1 vector. All constructs were verified by DNA sequencing. All constructs were verified by DNA sequencing.

Primary neuron culture and transfection

Primary rat hippocampal neurons derived from embryonic day 18 Sprague Dawley fetal rats of either sex were prepared as described previously²⁰. Briefly, hippocampi were dissected, dissociated with papain (Worthington Biochemical Corporation, Lakewood, NJ), and resuspended in minimal Eagle's medium (MEM, Invitrogen) supplemented with 0.6% glucose, 1 mM pyruvate, 2 mM L-glutamine, and 10% fetal bovine serum (Hyclone, South Logan, UT), and plated on poly-D-lysine-coated glass coverslips in 60 mm Petri dishes. Four hours after plating, the medium was replaced with a neurobasal medium (Invitrogen) supplemented with 2% NS21, 0.5 mM L-glutamine. Neurons were transfected by a modified calcium-phosphate method as previously described²⁰.

Chemically-induced long-term potentiation of hippocampal neurons

Transfected mature neurons (DIV 21) were preincubated with 50 μ M AP5 for 48 h in neurobasal media and transferred to a magnesium-free Tyrode's solution (119 mM NaCl, 2.5 mM KCl, 2 mM CaCl₂, 2 mM MgCl₂, 25 mM HEPES, pH 7.4 and 30 mM glucose. Images were acquired at 10 s intervals, and, after the second acquisition, cLTP-inducing solution (200 μ M glycine, 20 μ M bicuculline, 1 μ M strychnine, 0.5 μ M TTX in Mg²⁺ free Tyrode) was added for 3 min. The solution was changed to magnesium-free

Tyrode' s solution and the cells were imaged for an additional 4 min at 10 s intervals.

Classification of dendritic spines

Transfected neurons were rinsed with Tyrode' s solution and fixed with 4% paraformaldehyde (PFA) in 4% sucrose-containing 0.1 M phosphate-buffered saline (pH 7.3) (PBS) for 10 min at RT, then washed with PBS. Images were acquired with an inverted microscope (IX71, Olympus, Tokyo, Japan) equipped with an sCMOS camera (Zyla-5.5-CL3, Andor Technology, Belfast, Ireland). Well-branched pyramidal neurons were randomly selected, and the analysis was performed in a single-blinded manner. To categorize the spines, fluorescent images were imported into NeuronStudio²¹ for automated detection of dendrites and spines. Spine types were classified by measuring the aspect ratio, head-to-neck ratio, length, and spine head diameter of individual spines. Mushroom spines were defined as dendritic protrusions of around 1 μm in length with a head of width $> 0.6 \mu\text{m}$, while stubby spines had no distinguishable heads, as the head diameter was almost equal to the neck diameter, and length $w < 1 \mu\text{m}$. Spines with a head of width $< 0.6 \mu\text{m}$ and a length-to-head ratio of less than 2.5 were defined as thin spines. The spine head was defined as a tip structure at least 1.3 times thicker than the spine neck.

3D-structured illumination microscopy (SIM) imaging and data processing

After cLTP induction, neurons mounted in a chamber were imaged using an N-SIM microscope (ECLIPSE Ti-E, Nikon, Tokyo, Japan) equipped with an oil immersion TIRF objective lens (Apo TIRF 100

\times N.A. 1.49), and an EMCCD camera (iXon DU-897, Andor Technology). The lateral and axial resolutions measured using 100 nm diameter beads are 115 nm and 269 nm respectively in 3D-SIM mode. The acquired datasets, comprising 48 axial sections of 512×512 pixels, were computationally reconstructed using the reconstruction stack algorithm of NIS-Elements AR software (Nikon). The voxel size of the reconstructed images was 32 nm in the x- and y-dimensions and 120 nm in the z-dimension, with 16-bit depth. The reconstructed SIM image stacks were processed with DXplorer²².

Shape factor analysis

Changes in spine morphology were assessed from time-lapse images of shRNA-nArgBP2 with or without nArgBP2-*res* using the “Shape Descriptors” plug-in in Fiji. The form factor ($f = 4\pi A/p^2$) was calculated from the perimeter p and the area A of the object. The value approaches 1 as the spine head is rounder and 0 as the spine head is more irregular or elongated.

Western Blot and immunoprecipitation

Samples were lysed in 1% Triton-X 100 buffer (20 mM Tris pH 7.5, 137 mM NaCl, 10% glycerol, 1% Triton-X 100, 2 mM EDTA) in the presence of a protease inhibitor mixture (Roche), clarified by centrifugation at $13,200 \times g$ for 20 min and concentrations were measured with a Bicinchoninic acid (BCA) Protein Assay Reagent Kit (ThermoFisher, Waltham, MA). For immunoprecipitation experiments, ionomycin was treated before lysis and lysates were incubated with primary antibody at 4°C for 2 h and then 2 h after adding Protein A-Sepharose beads (GE Healthcare, Chicago, IL).

Then, samples were separated by SDS–PAGE gels and transferred to PVDF membranes (Merck, Burlington, MA). The membranes were blocked for 30 min with 5% (wt/vol) nonfat dry milk in TBST (10 mM Tris·HCl pH 7.6, 100 mM NaCl, 0.1% Tween 20) incubated with the primary antibodies overnight at 4° C and incubated with the corresponding HRP–conjugated secondary antibody for 1 h at room temperature. Chemiluminescence reactions were performed with an AbSignal Western detection kit system (AbClon, Seoul, South Korea) and acquired using an ImageQuant LAS 4000 (GE Healthcare).

Cell culture and transfection

COS7 cells were cultured at 37°C in 5% CO₂ in DMEM (Invitrogen, Carlsbad, CA) supplemented with 10% fetal bovine serum, and transfected with constructs using PEI (MW 4000) (Polysciences, Warrington, PA) at a ratio of 1:4 (total DNA (μ g) to PEI (μ L)).

Protein purification

All proteins were expressed in *Escherichia coli* BL21 (DE3). Cells were grown at 37 ° C in 2xYT medium with ampicillin (50 μ g/ml) to A₆₀₀ 0.6–0.8, followed by induction with 0.5 mM isopropyl– β –D–thiogalactopyranoside (IPTG) at 37° C for 4 h or at 16° C overnight. Cells resuspended in lysis buffer (25 mM HEPES [pH 7.4], 400 mM KCl, 20 mM imidazole, 10% glycerol, 0.5% Triton X–100, 1 mg/ml lysozyme, 0.1 mg/ml DNase I, 1 mM PMSF, protease inhibitor cocktail) were sonicated and rocked at 4° C for 1 h with 0.5% n–lauroylsarcosine sodium salt. After centrifugation, the supernatant was incubated with Ni–NTA chelating agarose beads (Incospharm, Daejeon, South Korea) at 4° C. Proteins were eluted

with a buffer containing 25 mM HEPES [pH 7.4], 300 mM imidazole, 1 mM DTT, and various concentrations of KCl. All proteins were quantified by SDS-PAGE.

***In vitro* droplet imaging**

Protein solutions were injected into a custom-made chamber assembled by attaching a cleaned 18 mm coverslip onto a glass slide. For CaMKII α *in vitro* droplet imaging, 1 μ M CaMKII α (Thermo) was incubated in CaMKII α activation buffer (50 mM Tris, pH 7.5, 10 mM MgCl₂, 2 mM DTT, 0.1 mM Na₂EDTA, 2 mM CaCl₂, 100 μ M ATP, 1.2 μ M calmodulin) for 10 min and then added to proteins. Images were acquired with a 488 or 561 nm laser using a spinning disk confocal microscope (ECLIPSE Ti-E, Nikon) with an oil immersion objective lens (Plan Apo 60 \times N.A. 1.40), and a Neo sCMOS camera (Andor Technology) at room temperature. Phase separation was noted by visual inspection and analysis using ImageJ software (NIH).

Quantification of droplet formation in COS7 cells

Average fluorescence intensity (intensity/cell area) values reflecting the expression level of the fluorescent protein in each cell were measured using ImageJ. The presence of droplets was assessed as follows: we first subtracted the background from each image and applied the threshold function to acquire a binarized image; then the number of droplets was quantified using the 'Analyze Particles' command. Droplets with a size $< 0.4 \mu\text{m}^2$ and with circularity < 0.8 were excluded [circularity = 4π (area/perimeter²); 1.0 = a perfect circle]. If the droplet count was < 5 , we visually examined the original image to ensure the presence

of droplets. The analysis was performed at least three times on a single-blind basis to ensure reproducibility.

FRAP assays

Experiments were performed using the stimulus-setting menu in the Nikon A1 to control sequential image acquisition using a 60X oil-immersion lens (1.40 N.A.) equipped with a Nikon A1 confocal microscope (Nikon) to accomplish photobleaching of a circular or cylindrical ROI by laser pulse emission. ROIs containing single droplets of COS7 cells were imaged every 5 s. After 5 images had been acquired, the droplet was photobleached for 2.5 s with a 488 nm laser (100%) and fluorescence recovery was imaged at 5 s intervals at 37° C. Average intensity values of ROI and total image fluorescence were obtained from each FRAP image using Nikon imaging software (NIS-elements). ROI values over time were plotted. Fluorescence intensities in the bleached ROIs were normalized to initial values.

Fluorescence live-cell imaging

Live cell images were acquired using a spinning disk confocal microscope (Nikon).

1,6-hexanediol treatment: COS7 cells and neurons in Tyrode' s solution were imaged at 5 s intervals and exposed to 3% 1,6-hexanediol (Sigma) in Tyrode' s solution.

Ionomycin: Time-lapse images of transfected COS7 cells were acquired for 1 min at 5 s intervals. After the third acquisition, ionomycin (Sigma) was added to a working concentration of 10 μ M.

Statistics

The normality of data was examined with the Kolmogorov–Smirnov normality test. Student’ s two–sample t –test was used to compare pair of independent groups and one–way ANOVA followed by Tukey’ s honest significant difference (HSD) post hoc test was used for multiple conditions. When the normality of data could not be assumed, the Kruskal–Wallis test was used for the nonparametric comparison of multiple groups. Prism 8 (GraphPad Software, San Diego, CA) was used for statistical analysis. The relevant p values are presented in the figure legends and, unless otherwise indicated, data are presented as means \pm s.e.m. (Standard Error of the Mean) or s.d. (Standard Deviation), with n indicating the number of independent experiments.

RESULTS

Knockdown of nArgBP2 does not induce any morphological abnormalities in the pre-existing dendritic spines of mature neurons. However, it completely impedes the enlargement of spines during chemically-induced long-term potentiation (cLTP)

As previously reported, I found that knockdown (KD) of nArgBP2 in developing neurons caused a drastic inhibition in the formation of mushroom-shaped dendritic spines and selective inhibition of excitatory spine-synapse formation (**Fig. 1a-b**)¹². Despite having such profound effects on developing neurons, however, I found that nArgBP2 KD in mature hippocampal neurons (KD at DIV 16 and observed at DIV 21; **Fig. 2**), did not result in any morphological defects in the existing dendritic spines (**Fig. 1b**). Indeed, the proportions of mushroom, stubby, and thin spines were similar in control and KD neurons.

To unravel the underlying mechanisms behind these seemingly contradictory findings in developing and mature neurons, I hypothesized that nArgBP2 might function when neurons undergo dynamic structural remodeling, such as during development or synaptic plasticity². To test this possibility, I induced glycine-induced chemical long-term potentiation (cLTP) in cultured mature neurons, which is known to activate synaptic NMDA receptors and induce the enlargement of dendritic spines^{23,24}. I found that cLTP induced a significant increase in the size of the spine heads in control neurons while it failed to do so in nArgBP2 KD neurons (**Fig.**

3a–b). In control neurons, the relative size of dendritic spines gradually increased for 30 min after induction of cLTP whereas in KD neurons it instead decreased (2.00 ± 0.13 for control, 0.96 ± 0.13 for KD). Expression levels of NMDA receptors, GluN1 and GluN2 were not altered with nArgBP2 KD (**Fig. 4**). The defect in spine enlargement was fully rescued by the expression of shRNA-resistant nArgBP2 (EGFP–nArgBP2–*res*), ruling out the off-target effects of shRNA expression (**Fig. 3a–b**).

To more accurately analyze the alteration in spine morphology in 3 dimensions (3Ds), I used DXplorer, a machine-learning-based 3D spine morphology analysis program that our lab including me recently developed by collaborating with colleagues²². I first acquired 3D spine images before and after cLTP using a structured illumination microscope (SIM) and extracted a set of morphological high-dimensional features from the 3D meshes of dendritic spines (**Fig. 5a**). I then measured the ratio of these values before and after cLTP (Post/Pre, **Fig. 5b–c**). The relative surface area after cLTP increased significantly in the control spines but decreased in the KD spines (S; 1.47 ± 0.09 for control, 0.93 ± 0.06 for shRNA, **Fig. 5c**). The volume of control spines doubled after cLTP but remained the same in KD spines (2.04 ± 0.24 for control, 1.01 ± 0.09 for shRNA, **Fig. 5c**). I further found that while the maximum neck diameters in control and KD neurons were similar, the ratio of maximum head diameter to neck diameter increased significantly in the controls, indicating that nArgBP2 functions as a spine-head expander (**Fig. 5c**). Thus, nArgBP2 KD in mature neurons had no effect on spine morphology in the resting state, but completely inhibited the enlargement of spine heads during cLTP, thus implying

that nArgBP2 is active during structural remodeling.

nArgBP2 forms condensates within dendritic spines, and these condensates undergo CaMKII α -mediated dispersion during cLTP and induce spine enlargement in living hippocampal neurons.

I next sought to find the underlying mechanism of nArgBP2-mediated spine enlargement during cLTP. To monitor nArgBP2 behaviors in living neurons, we first transfected hippocampal neurons with EGFP-tagged nArgBP2₉₅₉₋₁₁₉₆ and full-length nArgBP2-*res* in a nArgBP2 KD background to exclude the effect of endogenous nArgBP2. I confirmed that the expression of EGFP-nArgBP2-*res* in a KD background resulted in a comparable expression level to the endogenous nArgBP2 level (**Fig. 6**), and subsequent experiments in living neurons were performed using expression of shRNA-resistant forms in the background of KD (hereinafter only the construct name is referred to).

I found that EGFP-full-length nArgBP2 formed condensates that are located mostly in dendritic spines and partially in the shafts, consistent with previous studies on nArgBP2 localization in dendritic spines^{11,12}. Then, I induced glycine-induced cLTP in hippocampal neurons at DIV 21 (**Fig. 7**). I found that the EGFP-nArgBP2 condensates rapidly dispersed into the cytosol of the dendritic spines within a few minutes of cLTP induction while those in the dendritic shafts remained unaffected (**Fig. 7a**). More importantly, I found that condensate dispersion was accompanied by the expansion of the dendritic spine heads and there was a spatiotemporal correlation between them (**Fig. 7a, c**).

I further found that the above phenomena with full-length nArgBP2 were fully recapitulated by its SH3 domain mutant, nArgBP2₉₅₉₋₁₁₉₆. As observed with full-length, the EGFP-nArgBP2₉₅₉₋₁₁₉₆ condensates rapidly dispersed into the cytosol of the dendritic spines within a few minutes of cLTP induction (**Fig. 7b**). Furthermore, I found that EGFP-nArgBP2₉₅₉₋₁₁₉₆ condensate dispersion accompanies spine enlargement (**Fig. 7b, d**). These results indeed are consistent with previous results that SH3 domains are the self-functional modules that mediate the structural remodeling of dendritic spines¹². The overexpression of full-length nArgBP2 often caused large actin aggregates, which is consistent with the previous reports that nArgBP2 overexpression induced coalescence of F-actin into large aggregates due to N-terminal SoHo domain. To avoid this complication, I decided to use nArgBP2₉₅₉₋₁₁₉₆ in further experiments. I believe this alternative is legitimate given that the SH3 domain is the functional domain that drives structural remodeling in spines and behaves similarly to the full-length protein (**Fig. 7a-d**).

nArgBP2 condensates are dispersed by CaMKII α -mediated phosphorylation.

Calcium/calmodulin-dependent protein kinase II α (CaMKII α) is a key effector controlling spine enlargement and synaptic strength during LTP *in vitro* and *in vivo*²⁴⁻²⁶. Since nArgBP2 contains several putative CaMKII α -dependent phosphorylation sites (see below), and CaMKII α could be an effector to dissolve nArgBP2 condensates upon cLTP induction.

nArgBP2₉₅₉₋₁₁₉₆ is predicted to contain a consensus sequence for phosphorylation by CaMKII (RXXS/T) at S1119 and two non-consensus sequences at S975 and S1179²⁷. Since all three residues are conserved among rat, human, and mouse SORBS2 (**Fig. 8a**), I decided to construct a phospho-deficient mutant in which S975, S1119, and S1179 were modified to alanine (3S3A) (**Fig. 8b**). I found that phospho-deficient EGFP-nArgBP2₉₅₉₋₁₁₉₆-3S3A also formed condensates in dendritic spines but remained assembled during cLTP and no spine expansion occurred (**Fig. 9a, c**). Accordingly, CaMKII inhibitor KN93 completely abolished EGFP-nArgBP2₉₅₉₋₁₁₉₆ dispersion and spine expansion (**Fig. 9b, d**). These results indicate that CaMKII α -mediated phosphorylation is required for the dispersion of nArgBP2 condensates and spine enlargement during cLTP.

Phase separation of nArgBP2 in heterologous and *in vitro* expression systems.

The dispersion of ArgBP2 condensates during cLTP suggests that these condensates are not solid-like aggregates but rather resemble liquid-like condensates caused by liquid-liquid phase separation (LLPS)^{28,29}. Indeed, nArgBP2 condensates in spines spontaneously fused with each other (**Fig. 10a, b**), and were dispersed by 3% 1,6-hexanediol (1,6-HD), alcohol known to disperse a variety of biomolecular condensates formed by LLPS via a mechanism that involves its hydrophobicity^{30,31} (**Fig. 11a-e**). I further found that endogenous nArgBP2 also formed condensates in spines that were dispersed by 1,6-HD (**Fig. 12**).

Recent studies have shown that LLPS is a means by which cells create membrane-less biomolecular droplets with broad regulatory properties. LLPS enables the spatial confinement of signaling effectors within complexes, thereby finely modulating their activity spatiotemporally³²⁻³⁴. A key feature of proteins that undergo LLPS is their ability to engage in multivalent, low-affinity interactions, either through intrinsically disordered regions or through association with binding partners¹⁸. Since nArgBP2 contains three SH3 domains and proline-rich domains (PRDs) in the C-terminal region⁷, I tested whether nArgBP2 could form LLPS-mediated biomolecular condensates via its SH3-PRD interactions. I first transfected EGFP-tagged full-length nArgBP2, its three SH3 domains (nArgBP2₉₅₉₋₁₁₉₆), and nArgBP2 without SH3s (nArgBP2₁₋₉₅₈) into COS7 cells (**Fig. 13a**). Remarkably, EGFP-nArgBP2₉₅₉₋₁₁₉₆ formed large spherical droplets, much brighter than the surrounding cytoplasm, indicating that the droplets are enriched with SH3 domains whereas nArgBP2₁₋₉₅₈ did not. (**Fig. 13a**). Next, I found that EGFP-nArgBP2₉₅₉₋₁₁₉₆-5P5A, a mutant in which the 5 proline residues in the PRDs changed to alanines, thus cannot mediate the intermolecular interaction with SH3 domains, failed to form a dimer or co-assemble into droplets in COS7 cells (**Fig. 13b-e**). Together, these results indicate that biomolecular condensate formation of nArgBP2 is mediated by multivalent intermolecular interaction between SH3 domains and the PRDs.

I next sought to examine if nArgBP2 possessed the potential for phase separation *in vitro* by performing cell-free assays using purified protein. Both purified EGFP-full-length nArgBP2 and

mEGFP-nArgBP2₉₅₉₋₁₁₉₆ alone formed large spherical condensates that had phase-separated from the bulk solution (**Fig. 14a,c**). I showed the phase diagrams by performing the condensate formation assay with various concentrations and a crowding agent (5% PEG-8000). The number and size of phase-separated condensates increased in an EGFP-nArgBP2 and mEGFP-nArgBP2₉₅₉₋₁₁₉₆ concentration-dependent manner (**Fig. 14b, d**). Furthermore, when mEGFP-tagged nArgBP2₉₅₉₋₁₁₉₆ and mCherry-tagged nArgBP2₉₅₉₋₁₁₉₆ were mixed in a 1:1 ratio, they co-assembled forming droplets of both proteins (**Fig. 14e, f**). This observation suggested that nArgBP2₉₅₉₋₁₁₉₆ could form liquid droplets regardless of fluorescent tags.

I next assessed the liquid droplet-like properties of nArgBP2₉₅₉₋₁₁₉₆ condensates. They often mobilized and spontaneously fused upon encountering one another, forming larger condensates over time (**Fig. 15a-b**). Fluorescence recovery after photo-bleaching (FRAP) experiments showed that, upon photobleaching, the EGFP-nArgBP2₉₅₉₋₁₁₉₆ puncta recovered up to ~70% of the initial value within a few seconds (**Fig. 15c-d**), indicating the liquid nature within condensates and a dynamic exchange with the surrounding cytoplasm. I further found that nArgBP2₉₅₉₋₁₁₉₆ droplets dissolved within a few seconds when exposed to 3% 1,6-HD (**Fig. 15e**). Experiments with purified mEGFP-nArgBP2₉₅₉₋₁₁₉₆ *in vitro* also showed that mEGFP-nArgBP2₉₅₉₋₁₁₉₆ condensates were dispersed with 1,6-HD (**Fig. 15f**). Besides, the number and size of droplets were reduced as the salt concentration was increased, indicating that electrostatic interactions were involved in the formation of droplets (**Fig. 15g**). The nArgBP2₉₅₉₋₁₁₉₆ condensates thus

displayed all characteristic features of LLPS in living cells as well as *in vitro*.

Dispersion of nArgBP2 condensates by Ca^{2+} /CaMKII α –mediated phosphorylation

I showed that CaMKII α –mediated phosphorylation is required for the dispersion of nArgBP2 condensates in the spines of living neurons (**Fig. 7, 9**). To further confirm this in the heterologous expression system, I co–expressed EGFP–nArgBP2_{959–1196} and SBFP2–tagged CaMKII α in COS7 cells and found that they were co–assembled into condensates. We found that activation of CaMKII α by elevating cytosolic Ca^{2+} with ionomycin induced rapid and complete dispersion of nArgBP2_{959–1196} droplets (**Fig. 16a–c**). No effect was observed in the absence of CaMKII α or extracellular Ca^{2+} (**Fig. 16a**). The phospho–deficient nArgBP2_{959–1196}–3S3A mutant also formed liquid droplets but these droplets were not dispersed by ionomycin treatment, even when co–expressed with CaMKII α (**Fig. 16d–f**), which is consistent with the results in living neurons (**Fig. 9a, c**). The phospho–mimetic nArgBP2_{959–1196}–3S3D mutant in which three putative CaMKII phosphorylation sites were modified to aspartic acid (3D) failed to form condensates at all (**Fig. 16d–e**). CaMKII inhibitor KN93 also abolished the dispersion of EGFP–nArgBP2_{959–1196} condensates by ionomycin (**Fig. 16f**). Taken together, these results strongly suggest that nArgBP2 nArgBP2_{959–1196} droplets are significantly collapsed by CaMKII α –mediated phosphorylation upon Ca^{2+} influx.

The purified nArgBP2_{959–1196} also formed liquid droplets, but upon

treatment of CaMKII α and ATP in the presence of calcium and calmodulin, these droplets were not dissolved but the fluorescence translocated to the periphery, forming phase-in-phase assembly (**Fig. 16g-i**). This is reminiscent of the previous finding that CaMKII and GluN2Bc in the condensates move to the periphery forming a distinct phase-in-phase assembly via a Ca²⁺/CaMKII-dependent manner *in vitro*³⁵.

nArgBP2 condensates are inhibited by binding protein WAVE1

I showed that nArgBP2 forms LLPS-mediated biomolecular condensates via its SH3-PRD interactions. The interaction between WAVE1-PRDs and nArgBP2-SH3 domains might compete with SH3-PRD-mediated self-oligomerization and phase separation of nArgBP2 as the PRDs of WAVE1 also binds to the first and second SH3 domains of nArgBP2 (**Fig. 17c**).

To test this hypothesis spatiotemporally, I took advantage of a photo-activated system to control phase transitions using the photolyase homology region (PHR) of *Arabidopsis thaliana* CRY2^{19,36}. CRY2-PHR undergoes reversible homo-oligomerization and dissociation upon exposure to blue light and the absence of blue light, respectively (**Fig. 17a**). I, therefore, fused nArgBP2₉₅₉₋₁₁₉₆ to CRY2 and expressed nArgBP2₉₅₉₋₁₁₉₆-mCh-CRY2 in COS7 cells (**Fig. 17a, b**). I confined the analysis to early-transfected cells in which obvious droplets had not formed in advance. Upon exposure to blue light, nArgBP2₉₅₉₋₁₁₉₆-mCh-CRY2 formed distinct large fluorescent clusters (**Fig. 17b**). These clusters persisted after removal of the blue light, suggesting that nArgBP2₉₅₉₋₁₁₉₆-mCh-

CRY2 formed condensed droplets (**Fig. 17b**). Then, nArgBP2₉₅₉₋₁₁₉₆-mCh-CRY2 and EGFP-WAVE1 were co-expressed in COS7 cells and I analyzed the correlation between nArgBP2₉₅₉₋₁₁₉₆ droplet size and the level of expression of WAVE1 (**Fig. 17c-e**). I found that the higher the levels of WAVE1 expression, the smaller the nArgBP2₉₅₉₋₁₁₉₆-mCh-CRY2 droplets formed upon blue light stimulation, suggesting that interaction nArgBP2₉₅₉₋₁₁₉₆ with WAVE1 interferes with the coacervation of cytosolic nArgBP2₉₅₉₋₁₁₉₆ into phase-separated droplets, resulting smaller droplets (**Fig. 17d-e**). These results indicate that phase separation of nArgBP2, which relies on weak intermolecular interactions, could be effectively counteracted by the stronger binding of WAVE1. This is consistent with the previous study that WAVE1 is preferentially associated with monomers of ArgBP2³⁷.

Spine enlargement caused by nArgBP2 during cLTP is mediated by WAVE1 interaction

WAVE1 is known to direct signals through the Arp2/3 complex to regulate actin polymerization to manifest spine enlargement during cLTP^{38,39} and I previously showed that nArgBP2 regulates spine morphology via WAVE-dependent pathways^{7,12}. I thus hypothesized that the interaction between WAVE1 and nArgBP2 is required for spine enlargement during cLTP.

I first measured the shape factor of spines⁴⁰, which indicates the stability of actin cytoskeletons to test this hypothesis (**Fig. 18a-b**). Previously I demonstrated that the nArgBP2 KD in developing

neurons causes highly unstable actin dynamics^{7,12}. I transfected shRNA-nArgBP2 with or without nArgBP2-*res* and then induced cLTP at DIV21. We found wide fluctuations in the shape factor of KD spines, suggesting the highly unstable nature of KD spines while the shape factor value oscillates closer to 0.9 in KD+nArgBP2-*res* spines indicating that spines constantly maintained their rounder shapes in these cells (**Fig. 18a-b**).

To study the interaction between WAVE1 and nArgBP2 during cLTP, I decided to block the interaction between WAVE1 and nArgBP2₉₅₉₋₁₁₉₆ during cLTP. I used the “knock-sideway” strategy using mitochondria-targeting SH3-1/2 of nArgBP2 that I have established in the previous study (**Fig. 18d**)¹². Since the first and the second SH3 domains of nArgBP2 bind to WAVE, I previously found that mitochondria-targeting SH3-1/2 successfully sequesters WAVE from the cytosol to the mitochondria, thus preventing WAVE from interacting with its binding partners¹². In addition, to block the nArgBP2 oligomerization between mito-SH3-1/2 and nArgBP2₉₅₉₋₁₁₉₆, I used mito-nArgBP2_{959-1110-2P2A}, a mutant in which two proline residues in the proline-rich sequences were changed to alanines (**Fig. 18c**). I expect that ArgBP2 is released from the condensates during cLTP, but the released ArgBP2 cannot interact with WAVE1 because it is sequestered into the mitochondria due to its interaction with mito-SH3-1/2 (**Fig. 18d**). I transfected neurons with mTagBFP-tagged nArgBP2 shRNA, mCherry-nArgBP2₉₅₉₋₁₁₉₆, and EGFP-mito-nArgBP2_{959-1110-2P2A}, and induced cLTP at DIV 21 (**Fig. 18d-f**).

I found that blocking interaction with WAVE1 completely abrogated

the enlargement of the spine head upon cLTP (**Fig. 18e–f**). These results suggest that phase-separated nArgBP2 undergoes rapid CaMKII α -dependent dispersion during cLTP and, together with WAVE1, exhibits spine enlargement during synaptic plasticity (**Fig. 19**).

These results strongly suggest that the phosphorylation nArgBP2 serves as an inhibitory mechanism for its phase separation behavior. However, the interaction of phosphorylated nArgBP2 with WAVE1 should be maintained. These results necessarily imply that phosphorylation of nArgBP2 inhibits its phase separation, but the interaction of phosphorylated nArgBP2 with WAVE1 should be maintained. I tested whether CaMKII-mediated phosphorylation of nArgBP2 affects binding to WAVE1 (**Fig. 18g–h**). I have co-transfected HEK293T cells with CaMKII and either wildtype or phospho-deficient mutant (3S3A) of nArgBP2_{959–1196}, then treated cells with ionomycin and performed the co-immunoprecipitation experiment to compare the interaction between nArgBP2 and WAVE1 before and after ionomycin treatment (**Fig. 18g**). I found no difference in the interaction of nArgBP2 with WAVE1 between wildtype and phospho-deficient mutant regardless of ionomycin treatment (**Fig. 18h**), thus confirming that the interaction between nArgBP2 and WAVE1 is not affected by CaMKII-mediated phosphorylation.

nArgBP2 is characterized by the presence of a neuronal-specific exon (NSE) that is absent in ArgBP2 but the role of the NSE domain has not been studied. To investigate the function of NSE in nArgBP2, I transfected hippocampal neurons with GFP-tagged

nArgBP2 and nArgBP2 without the NSE domain. Whereas GFP–nArgBP2 recapitulated the distribution of endogenous nArgBP2 at dendritic spines, the GFP–nArgBP2 Δ NSE mutant localized at spines and dendritic shaft, suggesting that the NSE is required for the efficient targeting of nArgBP2 to the dendritic spines (**Fig. 21**). Also when hippocampal neurons were treated with a high concentration of zinc chloride, the localization of nArgBP2 changed. As GFP–nArgBP2 localized at both dendritic spines and shafts with a high concentration of zinc, I treated TPEN (N, N, N', N' –Tetrakis (2–pyridylmethyl)ethylenediamine) which is known as zinc chelator to observe zinc effect on the dendritic spine. As expected, nArgBP2 treated with zinc and TPEN, showed the same localization as control neurons (**Fig. 22**). Through this, it was found that the localization of nArgBP2 was dependent on zinc concentration. Taken together, these results indicate that additional studies on the role of NSE and zinc finger present in nArgBP2 are essential to further understand the role of nArgBP2 in neurons.

FIGURES

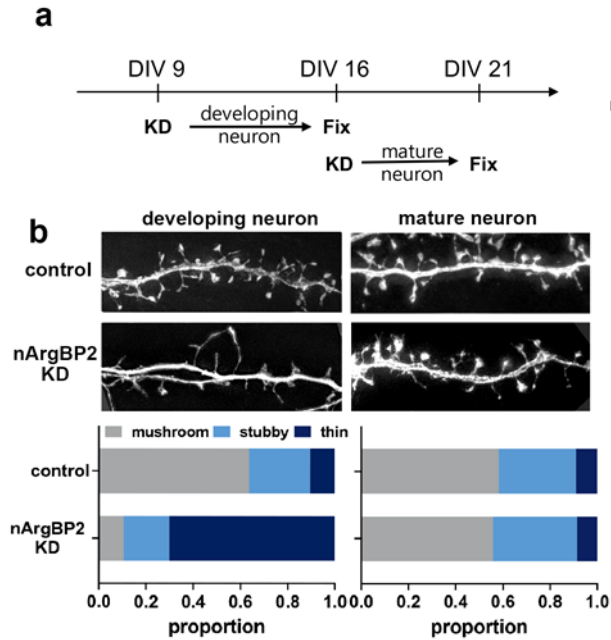


Figure 1. nArgBP2 KD in mature neurons does not result in morphological defects in existing dendritic spines. (a) Schematic overview of the nArgBP2 KD in developing and mature neurons (b) Representative images of spine morphologies and the proportions of mushroom-shaped, stubby, and thin spines in neurons expressing control or shRNA-nArgBP2 in developing neurons and mature neurons. Developing neurons were transfected at DIV 9 and fixed at DIV 16 whereas mature neurons were transfected at DIV 16 and fixed at DIV 21. Scale bar: 2 μ m. The proportion of each is shown above the bar.

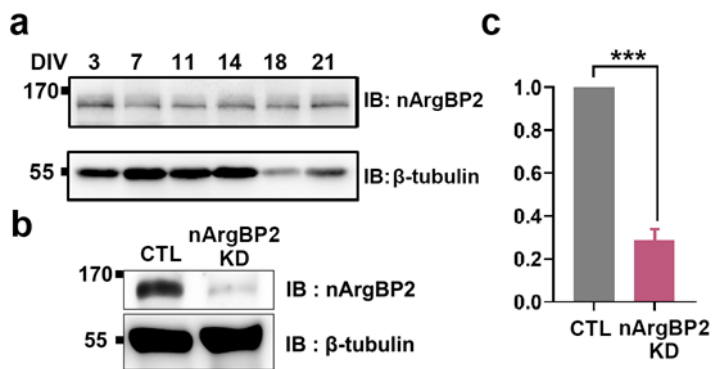


Figure 2. Sustained expression of nArgBP2 during neuronal development, and confirmation of knock-down efficiency by nArgBP2 shRNA. (a) Lysates from different developmental stages (DIV 3 - 21) were analyzed by Western blotting with anti-nArgBP2 antibody. β -tubulin served as a loading control. (b-c) Hippocampal neurons at DIV4 were infected with adeno-associated virus (AAV)-shRNA-nArgBP2 and the KD efficiency was confirmed by Western blotting with the anti-nArgBP2 antibody at DIV21. β -tubulin served as a loading control. ***p<0.001

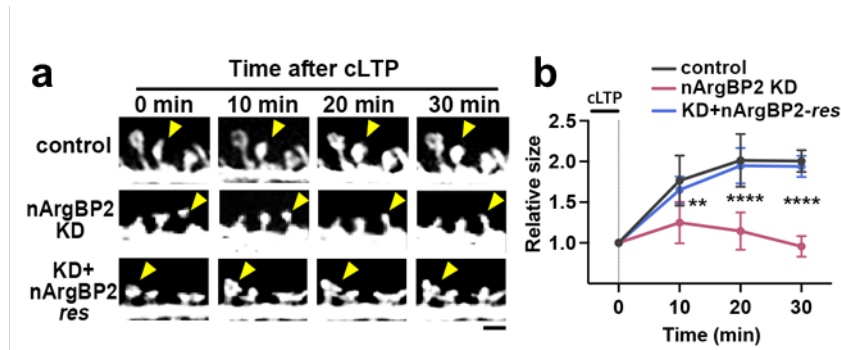


Figure 3. nArgBP2 KD in mature neurons completely inhibits spine head enlargement during cLTP. (a) Representative time-lapse images of spines in control and nArgBP2 KD neurons during cLTP induction. Neurons at DIV 16 were transfected with the shRNA-nArgBP2 alone, or combined with EGFP-nArgBP2-res, and were imaged at DIV 21. Note the gradual enlargement of the spine heads in control and KD+EGFP-nArgBP2-res neurons, but not in KD neurons. The yellow arrowheads indicate the spine heads. Scale bars: 2 μ m. (b) The relative size of spine heads in control and nArgBP2 KD neurons after cLTP, normalized to the initial value. $n = 9$ for control, 11 for KD, 7 for KD+EGFP-nArgBP2-res (One-way ANOVA followed by Tukey' s HSD test). * $p < 0.05$; ** $p < 0.01$. Error bars indicate means \pm s.e.m.

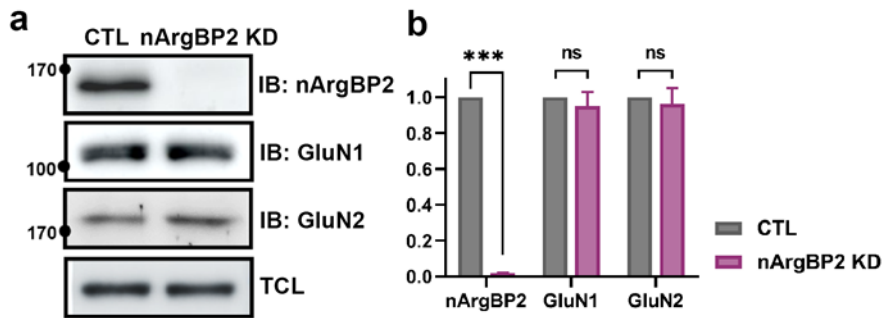


Figure 4. Expression levels of NMDA receptors, GluN1 and GluN2 were not altered with nArgBP2 KD in hippocampal neurons. (a) Hippocampal neurons at DIV14 were infected with adeno-associated virus (AAV)-shRNA-nArgBP2 and lysed at DIV21. Western-blot was performed with anti-nArgBP2, anti-GluN1 and anti-GluN2. IB, immunoblot; TCL, total cell lysates. (b) The relative intensity of western blot from (a). Student's *t*-test, $n=3$, n.s, not significant. *** $p<0.001$.

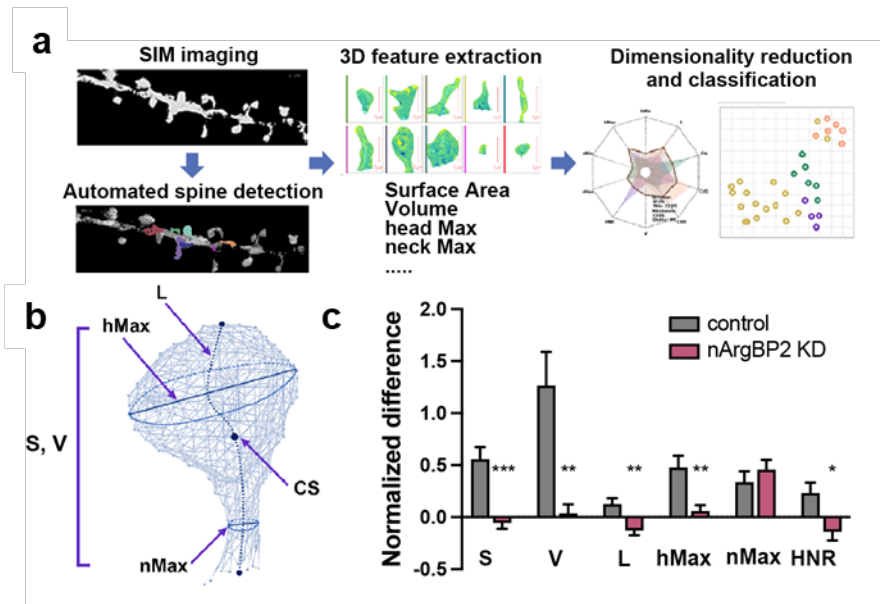


Figure 5. 3D geometry analysis of dendritic spines during cLTP. (a) Schematic diagram of the process of 3D geometry analysis of dendritic spines using DXplorer. Left panel shows the acquisition of 3D-SIM images and automatic detection of dendritic spines. 3D geometrical features were extracted and calculated. The data sets were further analyzed and classified by dimensionality reduction and machine-learning-based automatic classification. (b) Representative morphological features extracted from the 3D mesh of dendritic spines. S, Surface; V, Volume; L, length of spine; hMax, the maximum diameter of the spine head; nMax, the maximum diameter of the spine neck; CS, the centroid of the spine. (c) Normalized differences in morphological features of spines between pre- and post-cLTP in control and nArgBP2 KD neurons. HNR, the ratio of head to neck ($HNR = hMax / nMax$); $n = 39$ for control, 34 for KD. * $p < 0.05$; ** $p < 0.01$; *** $p < 0.001$. Student's t-test; Error bars indicate mean \pm s.d.

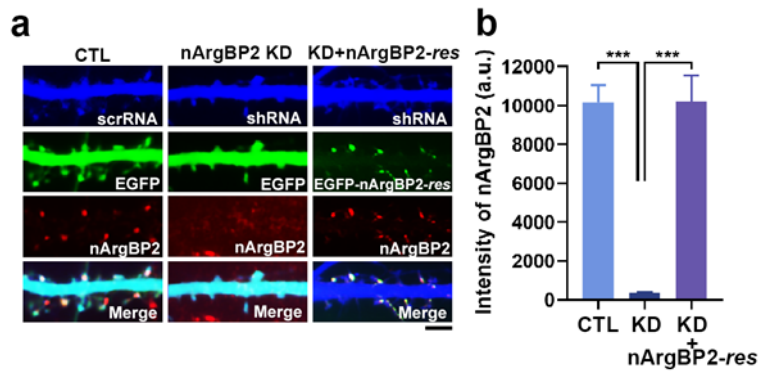


Figure 6. Expression of *nArgBP2-res* in ArgBP2 KD neurons showed similar expression levels to endogenous *nArgBP2* levels. (a) Representative images of dendrites of neurons co-expressing the scrambled-shRNA (scrRNA) with EGFP (left), shRNA with EGFP (middle), and with EGFP-*nArgBP2-res* (right) respectively. *res*, a silent mutation that is resistant to shRNA. (Scale bar: 10 μ m.) (b) The intensity of *nArgBP2* from (a) showed that expression levels of *nArgBP2-res* in *nArgBP2* KD was similar to endogenous *nArgBP2* levels. *** $p < 0.001$.

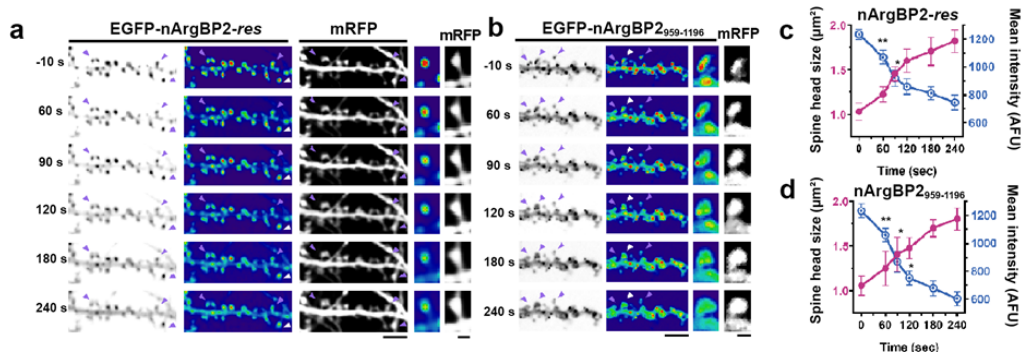


Figure 7. nArgBP2 forms condensates in the dendritic spines and these condensates are dispersed during chemical-LTP, which spatiotemporally coincides with spine head enlargement. Hippocampal neurons were transfected with EGFP-nArgBP2-*res*, EGFP-nArgBP2₉₅₉₋₁₁₉₆ and mRFP-tagged shRNA-nArgBP2 to exclude the effect of endogenous nArgBP2. **(a–b)** Representative time-lapse inverted images and pseudo-colored images of hippocampal neurons transfected with EGFP-nArgBP2-*res* **(a)**, EGFP-nArgBP2₉₅₉₋₁₁₉₆ **(b)**, upon cLTP stimulation. The third columns show magnified pseudo-colored views of the spines indicated by white arrowheads. The last columns show the mRFP signal in the spine cytosol used as a volume marker. Scale bars: 10 μ m and 1 μ m, respectively. **(c–d)** Plots of time-dependent changes in single spine head size and mean intensity of EGFP-nArgBP2-*res* **(c)**, EGFP-nArgBP2₉₅₉₋₁₁₉₆ **(d)** spines after cLTP, respectively. Both EGFP-nArgBP2-*res* and EGP-nArgBP2₉₅₉₋₁₁₉₆ in the dendritic spine dispersed rapidly during cLTP, leading to spine enlargement. See Methods for more details. n=10; *p < 0.05; **p < 0.01; The spines and droplets in the third columns of **(a)** and **(b)** were used for the analysis.

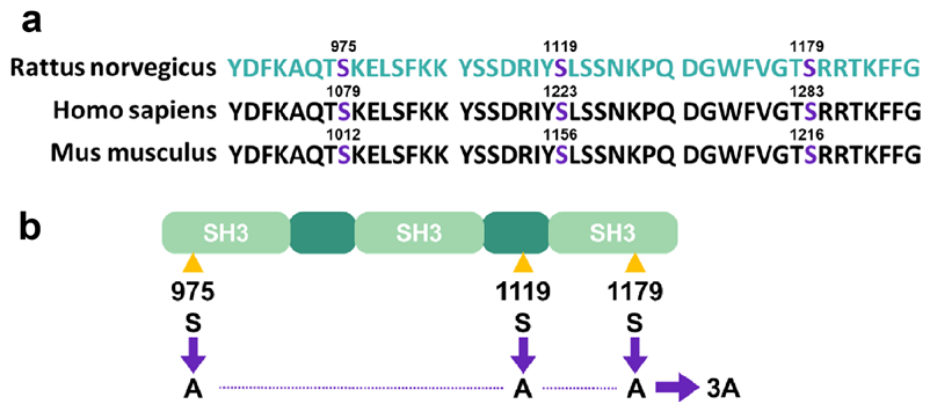


Figure 8. Conservation of putative CaMKII phosphorylation sites across species, and the schematic figure of CaMKII phosphorylation-deficient mutant (3S3A). (a) Multiple protein sequence alignment of nArgBP2 and orthologues from rat, human and mouse that are conserved. (b) Schematic diagram of nArgBP2₉₅₉₋₁₁₉₆-3S3A mutants.

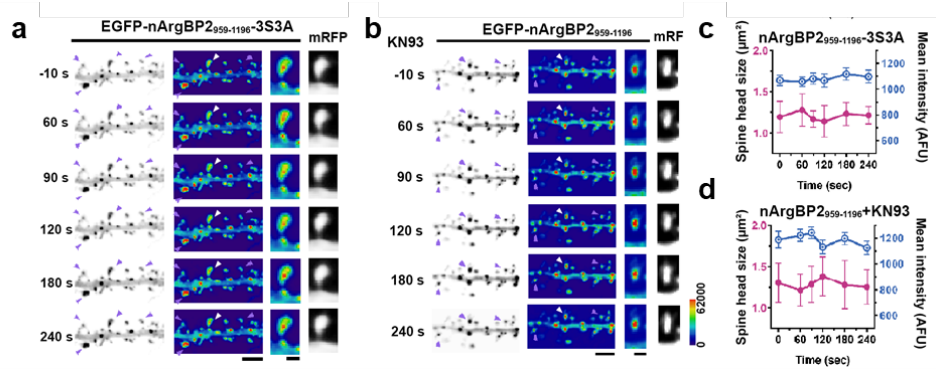


Figure 9. nArgBP2 forms condensates in the dendritic spines and these condensates are dispersed by CaMKII α -mediated phosphorylation. Hippocampal neurons were transfected with EGFP-nArgBP2₉₅₉₋₁₁₉₆ or EGFP-nArgBP2₉₅₉₋₁₁₉₆-3S3A and mRFP-tagged shRNA-nArgBP2 to exclude the effect of endogenous nArgBP2. **(a–b)** Representative time-lapse inverted images and pseudo-colored images of hippocampal neurons transfected with EGFP-nArgBP2₉₅₉₋₁₁₉₆-3S3A **(a)** or EGFP-nArgBP2₉₅₉₋₁₁₉₆ with KN93 treatment **(b)** upon cLTP stimulation. The third columns show magnified pseudo-colored views of the spines indicated by white arrowheads. The last columns show the mRFP signal in the spine cytosol used as a volume marker. Scale bars: 10 μ m and 1 μ m, respectively. **(c–d)** Plots of time-dependent changes in single spine head size and mean intensity of EGFP-nArgBP2₉₅₉₋₁₁₉₆-3S3A **(c)** and EGFP-nArgBP2₉₅₉₋₁₁₉₆ with KN93 treatment **(d)** spines after cLTP, respectively. Both EGFP-nArgBP2₉₅₉₋₁₁₉₆-3S3A and EGFP-nArgBP2₉₅₉₋₁₁₉₆ with KN93 treatment droplets in the dendritic spine didn't disperse during cLTP. See Methods for more details. n=10; *p < 0.05; **p < 0.01; The spines and droplets in the third columns of **(e)** and **(f)** were used for the analysis.

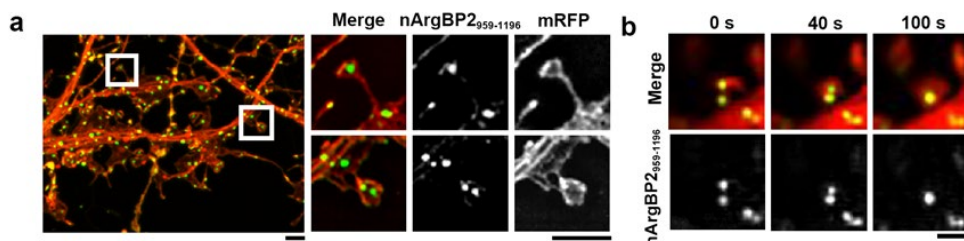


Figure 10. nArgBP2₉₅₉₋₁₁₉₆ droplets in living hippocampal neurons. Hippocampal neurons were transfected with EGFP-tagged nArgBP2₉₅₉₋₁₁₉₆ and mRFP-tagged shRNA-nArgBP2. **(a)** Representative images of nArgBP2₉₅₉₋₁₁₉₆ condensates in dendritic spines. **(b)** Representative fluorescence images of droplets that underwent fusion over time. Scale bars: 2 μm and 1 μm , respectively.

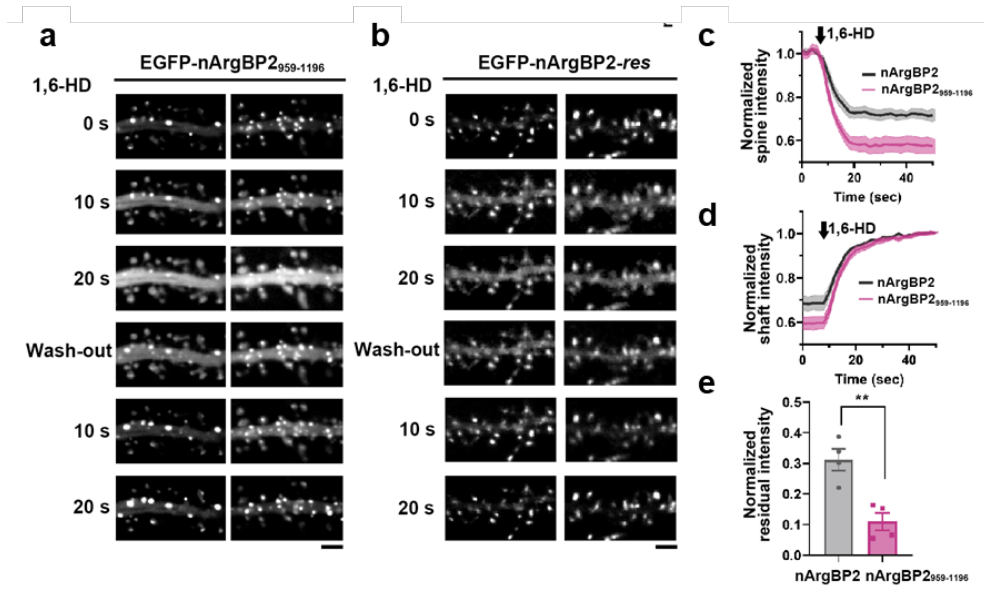


Figure 11. nArgBP2 droplets are dissolved by 1,6-hexanediol in living hippocampal neurons. (a-b) Time-lapse images of hippocampal neurons transfected with EGFP-tagged nArgBP2₉₅₉₋₁₁₉₆ (a), or EGFP-nArgBP2-res (b) and mRFP-tagged shRNA-nArgBP2 upon treatment with, and removal of, 3% 1,6-HD. Hippocampal neurons were transfected at DIV 16 and imaged at DIV 21. Scale bar: 10 μ m. (c-e) Plots of normalized fluorescence intensity traces of nArgBP2 and nArgBP2₉₅₉₋₁₁₉₆ droplets in the spine (c) and shaft (d) after 1,6-HD treatment. (e) The normalized residual intensity of nArgBP2 and nArgBP2₉₅₉₋₁₁₉₆ droplets after dispersion is complete (>30 sec). Fluorescence intensity of cytosol was subtracted from the intensity of the droplet. **p = 0.0044, Student's t-test; Error bars indicate mean \pm s.d.

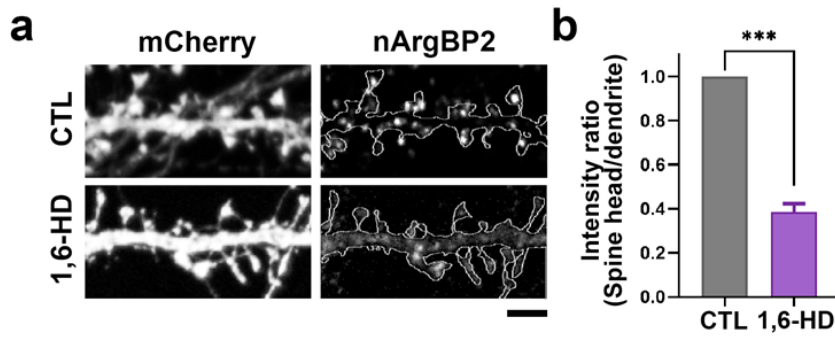


Figure 12. Endogenous nArgBP2 also formed liquid-like condensates in spines that were dispersed by 1,6-hexanediol treatment. (a) Hippocampal neurons were transfected with mCherry-C1 as a cytosolic marker and treated with 3% 1,6-hexanediol at DIV 21. Neurons were labeled with anti-nArgBP2. Scale bar : 2 μ m (b) Plot of nArgBP2 intensity ratio (Spine head/ dendrite). *** $p < 0.001$, Student' s t -test; Error bars indicate mean \pm s.d..

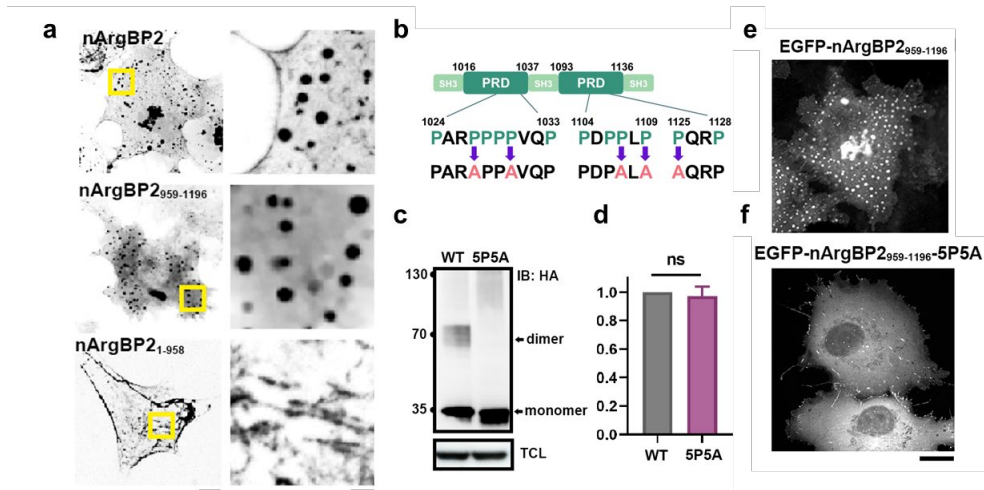


Figure 13. Biomolecular condensate assembly of nArgBP2 in heterologous systems with multivalent intermolecular interactions between SH3 domains and proline-rich domains. **(a)** Representative images of EGFP-tagged full-length nArgBP2, nArgBP2₉₅₉₋₁₁₉₆, and SH3 deletion mutant expressed in COS7 cells imaged at 48 h after transfection. Scale bar: 10 μ m. **(b)** Schematic diagram of nArgBP2₉₅₉₋₁₁₉₆ construct showing the proline-rich sequences between SH3 domains. P1027, P1030, P1107, P1109 and P1125 were each mutated to alanines (5P5A). **(c),(d)** Lysates from HEK293T cells transfected with HA-tagged nArgBP2₉₅₉₋₁₁₉₆ (WT) or nArgBP2₉₅₉₋₁₁₉₆-5P5A (5P5A) were treated with a cross-linking reagent (glutaraldehyde) and immunoblotted with anti-HA antibody. IB, immunoblot; TCL, total cell lysates. **(d)** Plot of the relative intensity of dimer and monomer of nArgBP2. Student's *t*-test; Error bars indicate mean \pm s.d. n.s, not significant. **(e),(f)** Representative fluorescence images of COS7 cells transfected with EGFP-nArgBP2₉₅₉₋₁₁₉₆ or EGFP-nArgBP2₉₅₉₋₁₁₉₆-5P5A. Scale bar: 20 μ m.

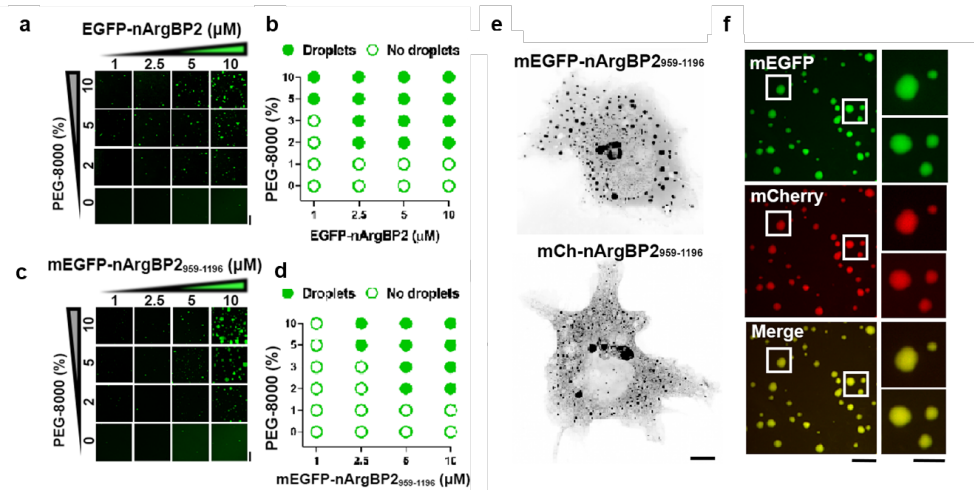


Figure 14 Biomolecular condensate assembly of nArgBP2 *in vitro* and heterologous systems (a–d) Fluorescence images of purified EGFP–nArgBP2 or mEGFP–nArgBP2_{959–1196} over a range of protein concentrations with or without the crowding agent, PEG–8000. Note that the formation of droplets is facilitated, and the size of droplets increases as the concentration of protein or PEG–8000 increases. Scale bar: 20 μ m. (b and d) Phase diagram showing droplet formation by EGFP–nArgBP2 (b) and mEGFP–nArgBP2_{959–1196} (d) with PEG–8000 *in vitro*. Filled circles indicate that mEGFP–nArgBP2_{959–1196} formed liquid droplets via LLPS, while empty circles indicate that did not. (e) Representative inverted images of mEGFP–tagged and mCherry–tagged nArgBP2_{959–1196} expressed in COS7 cells. Scale bars: 10 μ m. (f) Fluorescence images of purified mEGFP–nArgBP2_{959–1196} and mCherry–nArgBP2_{959–1196} colocalized in droplets. 5 μ M of each construct was mixed in a 1:1 molar ratio with 5 % PEG–8000. Scale bars: 20 μ m and 10 μ m, respectively.

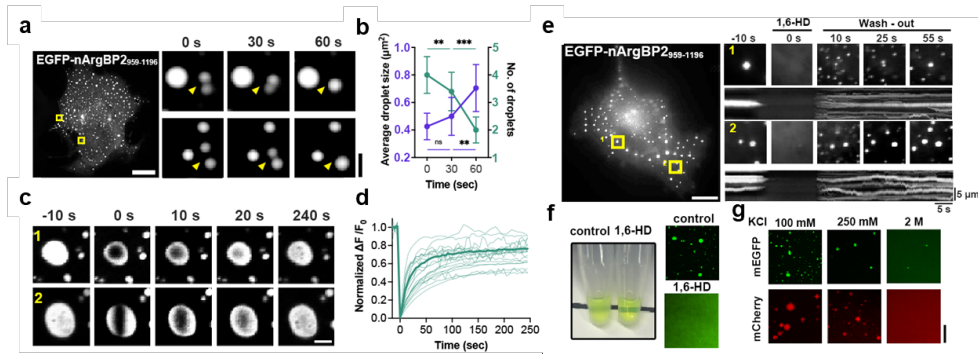


Figure 15. Biomolecular condensate assembly of nArgBP2 in heterologous and *in vitro* expression systems shows liquid-like properties. (a–e) COS7 cells were transfected with EGFP–nArgBP2_{959–1196} and imaged after 48 h. (a) Representative fluorescence images of droplets that underwent fusion over time (yellow arrowheads). Scale bars: 20 μ m and 2 μ m, respectively. (b) Time–dependent changes in the number and average size of droplets. n = 10 (0, 30 and 60 s) cells from 3 independent assays. Average droplet size, 0 s = 0.43 ± 0.09 ; 30 s = 0.50 ± 0.13 ; 60 s = 0.70 ± 0.17 ; values are means \pm s.d. One–way ANOVA followed by Tukey’ s HSD test. 0 s & 60 s ***p=0.0003, 30 s & 60 s **p=0.0070. (c) Representative time–lapse images showing fluorescence recovery after photobleaching of EGFP–nArgBP2_{959–1196} droplets. Either round or cylindrical–shaped bleached areas were created. Scale bar: 2 μ m. (d) Plots of normalized fluorescence intensity traces after photobleaching of multiple droplets. Average fluorescence intensity was traced as a thick line (n= 22). (e) Droplets are reversibly dispersed by 3% 1,6–hexanediol. Right: time–lapse images and kymographs of EGFP–nArgBP2_{959–1196} droplets are indicated by yellow rectangles in the low \–magnification image. Scale bar: 20 μ m. (f) Droplets of EGFP–nArgBP2_{959–1196} was dissolved by the addition of 10% 1,6–hexanediol (1,6–HD). (Top) The solution of purified EGFP–

nArgBP2₉₅₉₋₁₁₉₆, which had been turbid due to phase separation, became clear after adding 1,6-HD. (*Bottom*) Fluorescence images of purified EGFP-nArgBP2₉₅₉₋₁₁₉₆ with or without 1,6-HD. Scale bar: 20 μm . (**g**) Fluorescence images showing the effect of salt concentration on nArgBP2₉₅₉₋₁₁₉₆ droplet formation. 5 μM of purified mEGFP or mCherry tagged nArgBP2₉₅₉₋₁₁₉₆ protein was dissolved in 5% PEG-8000 buffer (25 mM HEPES [pH 7.4] with various concentrations of KCl). Elevated KCl weakens droplet formation via LLPS. Scale bar: 20 μm .

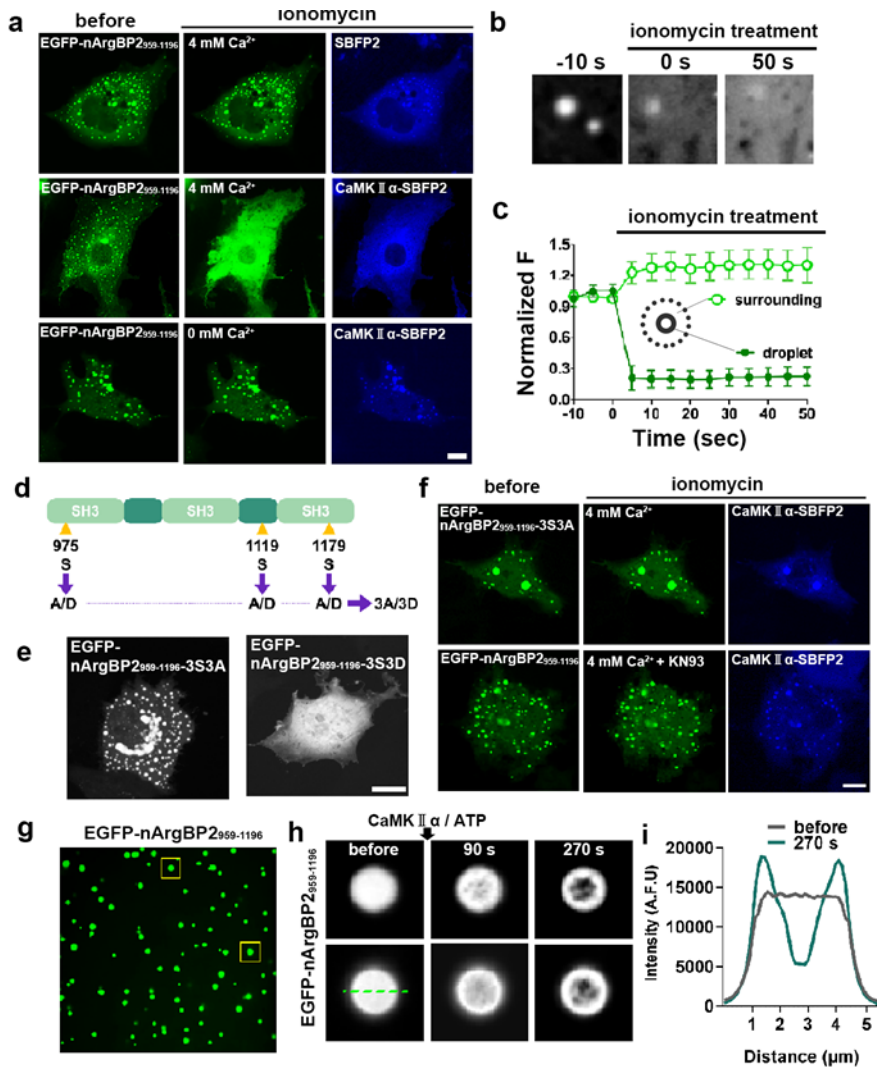


Figure 16. Biomolecular condensate co-assembly of nArgBP2 with CaMKII α and rapid dispersion by Ca²⁺/CaMKII α -mediated phosphorylation. (a) Representative fluorescence images of COS7 cells transfected with EGFP-nArgBP2₉₅₉₋₁₁₉₆ and SBFP2 empty vector or CaMK II α -SBFP2. EGFP-nArgBP2₉₅₉₋₁₁₉₆ droplets co-expressed with CaMK II α -SBFP2 dispersed upon ionomycin treatment in 4 mM Ca²⁺ Tyrode (middle), while no effect on the droplets was observed without CaMKII α co-expression (top) or in the absence of extracellular Ca²⁺ (bottom). Scale bar: 20 μ m. (b)

Enlarged time-lapse images of EGFP-nArgBP2₉₅₉₋₁₁₉₆ droplets co-expressed with CaMKII α -SBFP2 in the middle panel of (**Fig. 4a**) before and after ionomycin treatment. Scale bar: 1 μ m. (**c**) Plot of the normalized average fluorescence intensity profiles of EGFP-nArgBP2₉₅₉₋₁₁₉₆ droplets (filled circle) and surrounding cytosol (open circle) over time. n=54 for both droplets and surroundings. Values are means \pm s.d. (**d**) Schematic diagram of nArgBP2₉₅₉₋₁₁₉₆-3S3D (phospho-mimetic) and nArgBP2₉₅₉₋₁₁₉₆-3S3A (phospho-deficient) mutants. (**e**) Representative fluorescence images of COS7 cells transfected EGFP-nArgBP2₉₅₉₋₁₁₉₆-3S3D and EGFP-nArgBP2₉₅₉₋₁₁₉₆-3S3A. Scale bar: 20 μ m. (**f**) Representative fluorescence images of COS7 cells co-transfected with EGFP-nArgBP2₉₅₉₋₁₁₉₆-3S3A and CaMKII α -SBFP2, treated with ionomycin or KN93 and ionomycin in the presence of 4 mM Ca²⁺. Scale bar: 20 μ m. (**g**) Fluorescence images of purified EGFP-nArgBP2₉₅₉₋₁₁₉₆ before treatment of CaMKII α and ATP. (**h**) Enlarged time-lapse images of purified EGFP-nArgBP2₉₅₉₋₁₁₉₆ (yellow squares in **g**) before and after treatment of CaMKII α and ATP. Scale bar: 2 μ m. (**i**) Line scan plots of EGFP-nArgBP2₉₅₉₋₁₁₉₆ (green dashed line in **h**) fluorescence intensity before and after CaMKII α and ATP treatment.

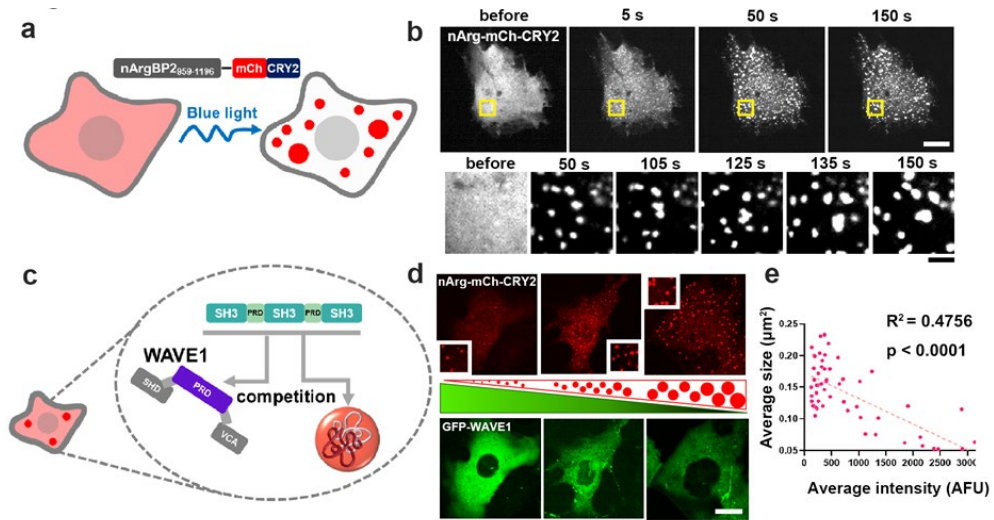


Figure 17. WAVE1 binds to nArgBP2 and their interaction interferes with the phase-separating property of nArgBP2. (a) Schematic figure of light-activated nArgBP2₉₅₉₋₁₁₉₆-mCh-CRY2. (b) Representative time-lapse fluorescence images of the light-activated assembly of nArgBP2₉₅₉₋₁₁₉₆-mCh-CRY2. COS7 cells were transfected with nArgBP2₉₅₉₋₁₁₉₆-mCh-CRY2 and stimulated with a 488 nm laser. Below: magnified images of the region enclosed by yellow rectangles in the low magnification images. Scale bars: 20 μm and 2 μm , respectively. (c) Schematic figure showing the interaction between WAVE1-PRDs and nArgBP2-SH3 domains competing with SH3-PRD-mediated self-oligomerization and phase separation of nArgBP2. (d) Representative fluorescence images of COS7 cells showing light-activated nArgBP2₉₅₉₋₁₁₉₆-mCh-CRY2 droplet formation at different levels of expression of EGFP-WAVE1. COS7 cells were co-transfected with nArgBP2₉₅₉₋₁₁₉₆-mCh-CRY2 and EGFP-WAVE1 and stimulated with blue light to induce nArgBP2₉₅₉₋₁₁₉₆-mCh-CRY2 droplets. Schematic triangular figures in the center illustrate the increase in the size of nArgBP2₉₅₉₋₁₁₉₆ droplets (red dots) and the decrease in WAVE1

expression levels (green). Scale bar: 20 μm . **(e)** Correlation between relative fluorescence intensity (which reflects expression level) of EGFP-WAVE1 and the average size of light-activated nArgBP2₉₅₉₋₁₁₉₆-mCh-CRY2 droplets. (n = 55, R² = 0.4756, p < 0.001).

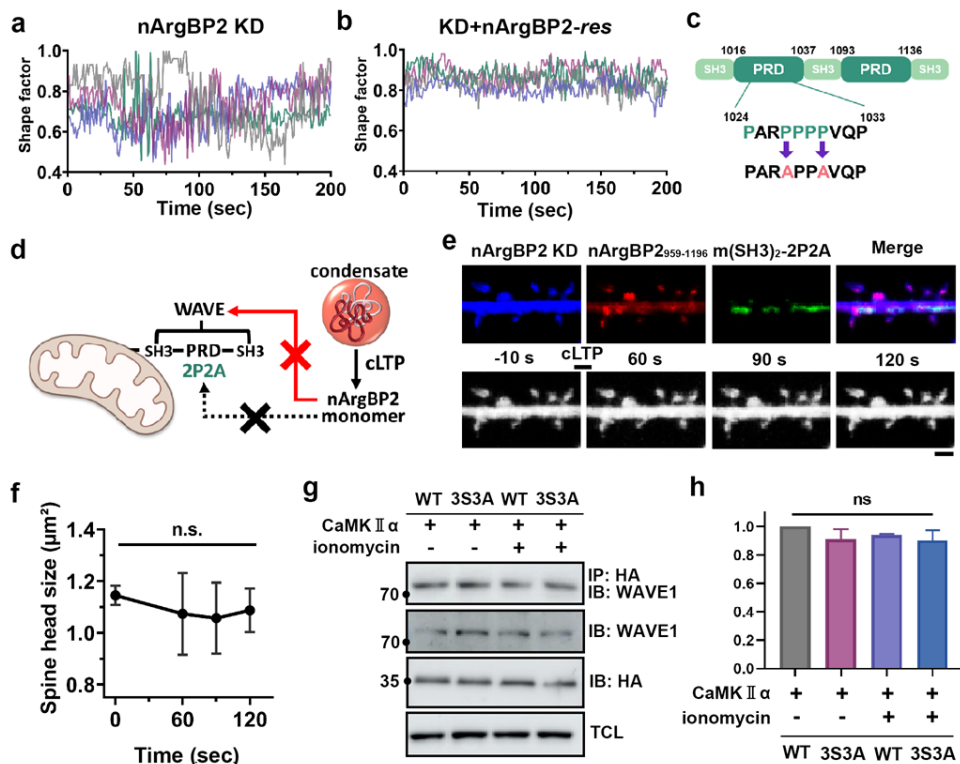


Figure 18. Spine enlargement caused by nArgBP2 during cLTP is mediated by WAVE1 interaction. (a–b) Hippocampal neurons were transfected with shRNA–nArgBP2 with or without nArgBP2–res. The shape factor of dendritic spines was calculated from time–lapse recordings during cLTP. Changes in shape factor which is the index of the spine motility were analyzed with the Form factor ($sf = 4\pi A/p^2$) plug–in of Fiji. Representative shape factor profiles of nArgBP2 KD and KD+nArgBP2–res spines during cLTP. Each color indicates an individual spine. (c) Schematic diagram of the mito–nArgBP2_{959–1196}–2P2A in which 2 proline residues (P1027 and P1030) were mutated to alanines (2P2A). (d–f) Hippocampal neurons were transfected with mTagBFP tagged shRNA–nArgBP2, mCh–nArgBP2_{959–1196}, and EGFP–mito–nArgBP2_{959–1110}–2P2A to sequester WAVE from the cytosol to the mitochondria. cLTP was induced at DIV 21. (d) Schematic figure of “knock–sideway”

strategy using mitochondria-targeting SH3-1/2 (nArgBP2₉₅₉₋₁₁₁₀)

(e) Representative fluorescence image of hippocampal neurons and time-lapse images upon cLTP. Scale bar: 2 μ m. **(f)** The plot of time-dependent changes in single spine head size upon cLTP. n=6, n.s., not significant.

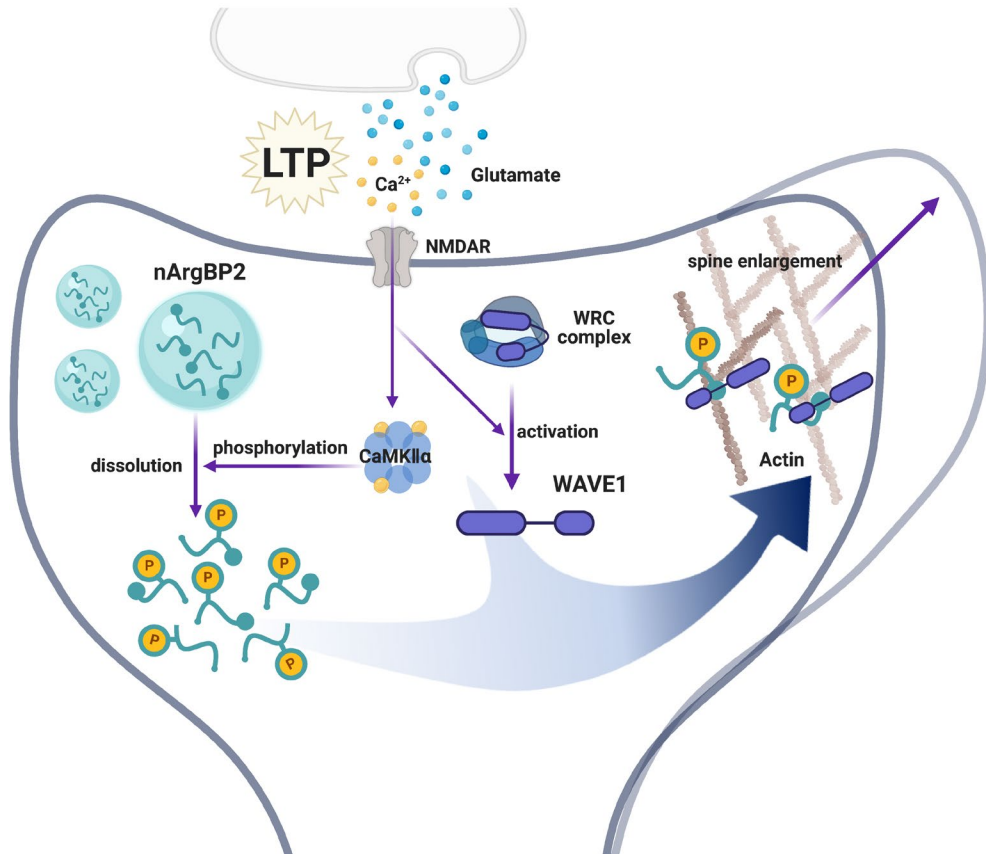


Figure 19. Model for the role of nArgBP2 in enlargement of dendritic spines during LTP. nArgBP2 at rest remains dormant by being sequestered in liquid droplets while WAVE1 also remains inactive by forming the WRC. Upon LTP induction, nArgBP2 is released from the droplets by calcium/calmodulin–dependent protein kinase II (CaMKII)–mediated phosphorylation, and WAVE1 is also released by the activated Rac1 and other kinases, thus two proteins now can interact with each other to regulate actin cytoskeletons and manifest the structural plasticity in dendritic spines. The schematic figure was created with Biorender.com.

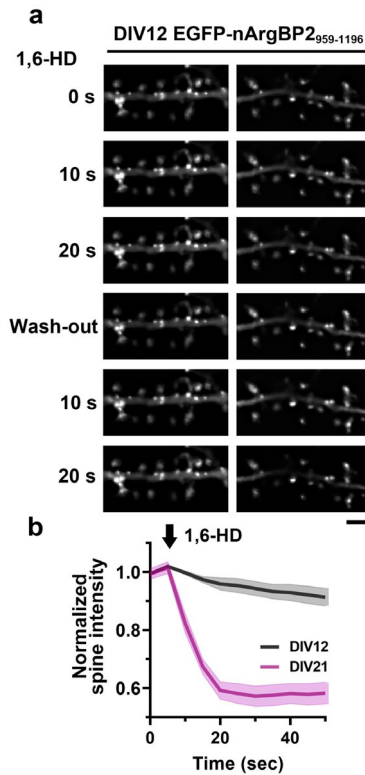


Figure 20. nArgBP2₉₅₉₋₁₁₉₆ also formed droplets in developing neurons but these droplets are reluctant to be dissolved by 1,6 hexanediol treatment. Hippocampal neurons were transfected with EGFP-tagged nArgBP2₉₅₉₋₁₁₉₆ and mRFP-tagged shRNA-nArgBP2 at DIV7 and imaged at DIV12. **(a)** Representative time-lapse image of nArgBP2₉₅₉₋₁₁₉₆ condensates upon treatment with, and removal of, 3% 1,6-HD. Scale bar: 10 μ m. **(b)** Plots of normalized fluorescence intensity traces of nArgBP2₉₅₉₋₁₁₉₆ droplets in DIV12 and DIV21 neurons after 1,6-HD treatment. The normalized residual intensity of DIV12 nArgBP2₉₅₉₋₁₁₉₆ droplets after 40 s dispersion is 0.92 ± 0.07 . n=3

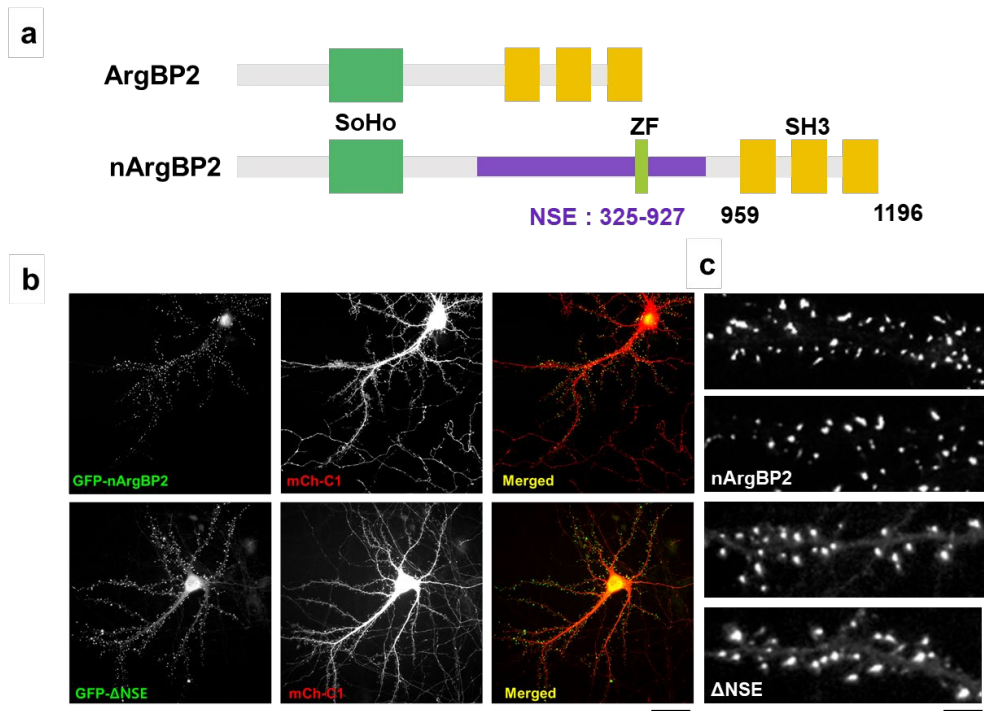


Figure 21. The NSE domain of nArgBP2 is required for the efficient targeting of nArgBP2 to dendritic spines. (a) Schematic figure of ArgBP2 and nArgBP2 (b) Distribution of exogenous GFP-nArgBP2 and GFP-nArgBP2 Δ NSE in cultured hippocampal neurons. (c) Enlarged boxed regions highlight the enrichment of GFP-nArgBP2 at spines. Scale bar: 10 μ m

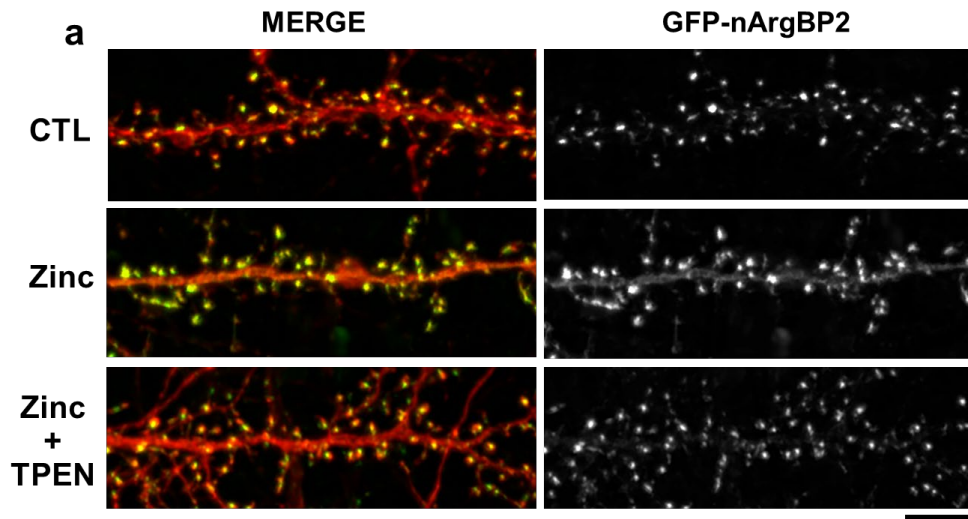


Figure 22. The efficient targeting of nArgBP2 to the dendritic spine is zinc-dependent. (a) Hippocampal neurons are transfected with GFP-nArgBP2 and mCherry-c1 at DIV 9. Distribution of exogenous GFP-nArgBP2 in cultured hippocampal neurons. Scale bar: 10 μ m

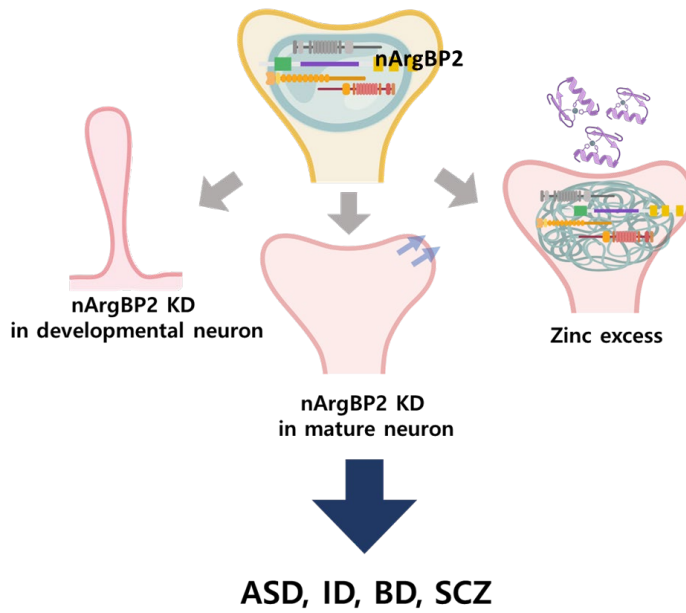


Figure 23. The schematic figure of role of nArgBP2.

DISCUSSION

The unique properties of condensed biological molecular droplets especially at synapses have been extensively studied in the last few years^{29,41-43}. However, most of the evidence for phase-separation-mediated synaptic assembly formation in those studies is based on *in vitro* studies, so the issue of whether it occurs in living neurons and has any physiological meaning remained questionable. Here, I provide compelling evidence that reversible phase-separation of postsynaptic nArgBP2 has a critical role in spine enlargement and structural plasticity in living neurons. These results further indicate that dynamic control of nArgBP2 liquid droplet formation and dispersion precisely coordinates the spatiotemporal interaction between nArgBP2 and WAVE1 in dendritic spines to induce spine enlargement during synaptic plasticity.

A series of recent studies have reported that the formation of condensed PSD, as well of presynaptic active zones, may involve phase-separation-mediated molecular assemblies^{29,41-43}. SynGAP has recently been shown to undergo LLPS and activity-dependent dispersion, which represents the initiation of LTP⁴⁴. The Fragile X Mental Retardation Protein (FMRP), an abundant RNA-binding protein in PSD, has been shown to phase separate *in vitro*, suggesting that LLPS of FMRP is a general mechanism implicated in activity-dependent translation and synaptic plasticity⁴⁵⁻⁴⁷. Moreover, reconstitution of PSD assembly using PSD-95, GKAP (also known as SAPAP), Shank, and Homer *in vitro* can generate highly-condensed assemblies via LLPS⁴², and these also

incorporate NR2B and SynGAP⁴². Further, the clustering of transmembrane AMPA receptor regulatory proteins (TARPs) into PSD condensates, which are essential for AMPA–receptor synaptic transmission in hippocampal neurons, is mediated via LLPS. Using an *in vitro* reconstitution approach, Wu *et al.* also demonstrated that the purified RIM and RIM–binding protein (RIM–BP) mixtures undergo phase separation and form presynaptic active zone–like condensates with voltage–gated Ca²⁺ channels²⁹. Synapsin 1, one of the most abundant proteins in presynaptic boutons, is also known to contain intrinsically disordered regions and forms phase–separated droplets *in vitro*^{41,48}. Thus, a distinctive feature of phase separation–mediated molecular assembly could provide a highly flexible and dynamic activity at synapses⁴³.

The SH3 domains of nArgBP2/ArgBP2 bind signaling protein kinases, the ubiquitin ligase, and proteins involved in the regulation of the actin cytoskeleton such as dynamin, synaptojanin, WAVE isoforms, and WAVE regulatory proteins⁷, suggesting that the SH3 domains appear to confer the most of known functionality of nArgBP2. Our lab also found that the SH3 domains of nArgBP2 sufficiently regulate the structural remodeling of dendritic spines¹². I also found that in the phase–separation context, the nArgBP2_{959–1196} behaves similarly to the full–length nArgBP2 in the physiological context of living neurons and COS–7 cells as well as *in vitro*.

Unlike *in vitro* results, however, in living fibroblasts, I did not find the segregation into phase–in–phase assembly but rather a rapid dissociation of droplets upon ionomycin treatment (**Fig. 16a–c**).

One plausible explanation for this difference could be attributed to the presence of other interacting molecules within cellular environments. Indeed, nArgBP2 engages in interactions with diverse molecular partners to fulfill its cellular functions in response to specific demands. Consequently, upon release, nArgBP2 is readily sequestered by these interacting molecules within the cellular milieu, leading to a reduction in the local concentration of free nArgBP2 and consequent dissolution of the condensates. In agreement with this context, I showed that the interaction between nArgBP2 and WAVE1 interferes with the phase-separating tendency of nArgBP2 (**Fig. 17**). I further showed that the interaction between nArgBP2 and WAVE1 is not affected by CaMKII-mediated phosphorylation. Since three putative CaMKII phosphorylation sites are in the first and third SH3 domains and second PRD domain (**Fig. 8**) while nArgBP2 interacts with WAVE1 via the first and second SH3 domains⁷, the second SH3 domain remains intact during cLTP-mediated phosphorylation, so it can regulate the interaction of nArgBP2 with WAVE1 even in the phosphorylated state. WAVE1 is also known to be autoinhibited as a component of the WAVE regulatory complex (WRC) at rest and upon activation of WRC by the Rac1, WAVE1 can interact with the actin to extend actin filaments⁴⁹. These results provide compelling evidence indicating that nArgBP2, during resting states, remains a dormant state through sequestration within liquid droplets, while WAVE1 remains inactive due to its association with the WAVE regulatory complex (WRC). The interaction between nArgBP2 and WAVE1 may not be realized until both proteins are released from their dormant states during long-term potentiation. Once activated, these two proteins synergistically coordinate actin polymerization in

dendritic spines, thereby facilitating structural remodeling processes (**Fig. 19**). Consequently, LLPS enables the timely transduction of signals during synaptic plasticity as a switch.

One of the remaining issues is the potential formation of condensates by nArgBP2 in developing neurons. Furthermore, if such condensates do form, an intriguing question arises regarding the underlying reasons why the ablation of nArgBP2 during the resting state elicits such significant effects on dendritic morphology, contrasting with the observed lack of morphological defects in mature neurons. I suggest that although nArgBP2 forms condensates in developing neurons, the high spontaneous activity and substantial structural remodeling during development skew its balance in the direction of either dissolution or solidification of condensates. Indeed, I found that nArgBP2₉₅₉₋₁₁₉₆ expressed in developing immature neurons does form condensates in spines but they often appear to be solid aggregates rather than liquid droplets showing only ~8% of fluorescence reduction upon 1,6-HD treatment (**Fig. 20**). Alternatively, it is plausible that the regulation of nArgBP2 condensate formation is governed by distinct mechanisms in developing and mature neurons. In this respect, it is worth noting that two major neuronal CaMKII isoforms α and β differ in cellular localization, spatiotemporal expression, and sensitivity to Ca²⁺ signals due to their different binding affinity for calmodulin⁵⁰⁻⁵². Indeed, CaMKII β is expressed⁵⁰⁻⁵² in the brain during early embryonic stages and development whereas CaMKII α predominates in juvenile stages up to maturity^{53,54}. This leads to the speculation that while CaMKII β phosphorylates nArgBP2 in the resting state during development, CaMKII α may act as a selective

synaptic tag during synaptic changes in mature neurons by phosphorylating nArgBP2 in response to Ca^{2+} influx. This idea deserves further study.

A previous study has reported the results of electrophysiological analysis on the LTP and LTD in the pan-Sorbs2 KO mice model¹¹. Whole-cell patch clamp recordings were conducted on dentate gyrus (DG) granule cells within acute brain slices obtained from 5-week-old knockout (KO) mice. It is known that the hippocampal DG receives inputs from the entorhinal cortex via two major paths, the medial performant path (MPP) and the lateral performant path (LPP). Zhang *et.al.* induced LTP/LTD at the outer one-third of the molecular layer in DG which is mainly innervated by LPP input from the lateral entorhinal cortex, and found that the properties of LTP and LTD were not altered in Sorbs2 KO compared to them in WT mice¹¹. Importantly, however, another study has found that immature neurons (4–6 weeks-old mice) do not reliably potentiate at LPP synapses but instead develop an increasingly greater capacity for LTP with age and neuronal maturity (over 3–4 months)⁵⁵. These results suggest that LTP at LPP synapses is weak in immature neurons and progressively increases with cell age over the course of several months. Besides, the LPP–DG synapse is known to usually express LTD or synaptic depression, and the MPP–DG synapse mainly expresses LTP⁵⁶. Since Zhang *et al.* used LPP synapses in young immature neurons (5 weeks old)¹¹, these could be the reason why they failed to observe the effect on LTP in young *Sorbs2* KO LPP synapses. Moreover, since it removes all *Sorbs2* isoforms, including nArgBP2, deficiency of all ArgBP2 isoforms in the nervous system can modulate neuronal function and

synaptic plasticity.

PSD-95, SAPAP, SHANK, and Homer which are major scaffolding components of PSD⁵⁷⁻⁶⁰ are individually relevant to various neuropsychiatric disorders associated with E/I imbalance, such as ASD (Autism Spectrum Disorder), ID, BD, OCD (Obsessive-compulsive disorder), and SCZ (Schizophrenia). All these diseases have complicated polygenic origins but are generally associated with a distinct pattern of dendritic spine pathology tightly linked to altered structural plasticity. Accordingly, numerous psychiatric disorders are characterized by dendritic abnormalities, including aberrant spine densities and morphologies, which probably affect excitatory drive and subsequent E/I balance in brain circuitry. Significantly, E/I imbalance caused by nArgBP2 deficiency is thought to underlie the synaptic dysfunction observed in BD and ID¹². These current results show that nArgBP2 regulates actin dynamics not only during spinogenesis in the early phase of neuronal development but also during the actin remodeling leading to the spine enlargement responsible for synaptic plasticity in mature neurons.

Data from large-scale studies have shown that a substantial number of individuals meet the criteria for two or more psychiatric disorders. For example, OCD is common among patients with BD^{61,62}, and a significant number of patients with ASD also have symptoms of BD⁶³. There is also a strong positive correlation between measures of depression and anxiety⁶⁴. Genome-wide genetic studies have identified overlapping risk genes across major psychiatric disorders, including SCZ, BD, major depressive disorder,

and ASD⁶⁵⁻⁶⁷. This indicates that dysregulation of single genes can cause different types of disorder depending on which particular protein network is disrupted. It is noteworthy that SHANK binds to the GH1 domain of SAPAP via its PDZ domain, and SAPAP in turn binds to the SH3 domain of nArgBP2 via its PRD. nArgBP2 and SHANK share a number of binding partners in the dendritic spines of excitatory synapses. It is thus tempting to speculate that nArgBP2, SAPAP and SHANK form a core scaffolding triad regulating the actin cytoskeleton in dendritic spines⁶⁸. Although the underlying molecular mechanisms that connect the aberrant expression of these genes and their behavioral consequences are still far from elucidated, phase-separation-mediated regulation of the activity of these proteins in dendritic spines has the potential to present novel avenues for comprehending the causal mechanisms that underlie neuropsychiatric disorders characterized by overlapping clinical symptoms.

nArgBP2 has a neuron-specific exon (NSE) absent in ArgBP2, however the role of the NSE domain has not been studied. I found that nArgBP2 Δ NSE mutant was less localized at spines, suggesting that NSE is required for nArgBP2 to efficiently localize at dendritic spines. Also, there is a zinc finger motif in the NSE domain of nArgBP2 and I showed that a high concentration of zinc ion disrupts nArgBP2 localization at the dendritic spine.

Zinc is known to be an important homeostatic component. Molecularly, zinc is a transcription factor that regulates gene expression and activates dozens of enzymes involved in neuronal metabolism. During development and adulthood, zinc acts as a

regulator of synaptic activity and neuroplasticity at the cellular level. Several neurological conditions can be affected by changes in zinc status, including stroke, neurodegenerative diseases, traumatic brain injury and depression. Therefore, zinc deficiency can lead to reduced cognitive and learning abilities and increased oxidative stress, and zinc accumulation can lead to neurotoxicity and neuronal cell death. Zinc-binding proteins require zinc for their structures and functions. For a number of cytoskeletal proteins, zinc fingers are shown to be sites of protein-DNA and protein-protein interaction. Also, the stability of the proteins significantly increases in the presence of an appropriate concentration of zinc. CTTNBP2 forms self-assembled condensates and facilitates SHANK3 co-condensation at dendritic spines. Zinc binds the N-terminal coiled-coil region of CTTNBP2, promoting higher-order assemblies.⁶⁹ Consequently, it leads to reduce CTTNBP2 mobility and enhance the stability and synaptic retention of CTTNBP2 condensates. Also, zinc fingers of Bassoon and Piccolo which are components of the presynaptic cytoskeletal matrix (PCM) may interact with vesicle-associated proteins in the presynapse, and potentially be involved in regulating the synaptic vesicle cycle^{70,71}. In addition to its role in regulating structural plasticity in mature neurons, it is expected to play a role in interaction with neuronal proteins through the NSE domain or in regulating zinc homeostasis by zinc fingers. I suggest the possibility of NSE of nArgBP2 regulating zinc-dependent plasticity or interaction with other synaptic proteins, which certainly is of interest for further study and it may provide new opportunities for understanding the mechanisms of zinc-related neuropsychiatric disorders.

REFERENCES

- 1 Arellano, J. I., Benavides–Piccione, R., Defelipe, J. & Yuste, R. Ultrastructure of dendritic spines: correlation between synaptic and spine morphologies. *Front Neurosci* **1**, 131–143, doi:10.3389/neuro.01.1.1.010.2007 (2007).
- 2 Bosch, M. *et al.* Structural and molecular remodeling of dendritic spine substructures during long–term potentiation. *Neuron* **82**, 444–459, doi:10.1016/j.neuron.2014.03.021 (2014).
- 3 Rossi, M. R. *et al.* Clinical and genomic characterization of distal duplications and deletions of chromosome 4q: study of two cases and review of the literature. *Am J Med Genet A* **149A**, 2788–2794, doi:10.1002/ajmg.a.33088 (2009).
- 4 Kawabe, H. *et al.* nArgBP2, a novel neural member of ponsin/ArgBP2/vinexin family that interacts with synapse–associated protein 90/postsynaptic density–95–associated protein (SAPAP). *J Biol Chem* **274**, 30914–30918 (1999).
- 5 Wang, B., Golemis, E. A. & Kruh, G. D. ArgBP2, a multiple Src homology 3 domain–containing, Arg/Abl–interacting protein, is phosphorylated in v–Abl–transformed cells and localized in stress fibers and cardiocyte Z–disks. *J Biol Chem* **272**, 17542–17550 (1997).
- 6 Kioka, N., Ueda, K. & Amachi, T. Vinexin, CAP/ponsin, ArgBP2: a novel adaptor protein family regulating cytoskeletal organization and signal transduction. *Cell Struct Funct* **27**, 1–7 (2002).
- 7 Cestra, G., Toomre, D., Chang, S. & De Camilli, P. The Abl/Arg substrate ArgBP2/nArgBP2 coordinates the function of multiple regulatory mechanisms converging on the actin cytoskeleton. *Proc Natl Acad Sci U S A* **102**, 1731–1736, doi:10.1073/pnas.0409376102 (2005).
- 8 Roignot, J. & Soubeyran, P. ArgBP2 and the SoHo family of adapter proteins in oncogenic diseases. *Cell Adh Migr* **3**, 167–170 (2009).
- 9 Feng, G. Genes and pathways involved in bipolar disorder. United States patent US20100077493 A1 (2010).

- 10 Schluth–Bolard, C. *et al.* Breakpoint mapping by next generation sequencing reveals causative gene disruption in patients carrying apparently balanced chromosome rearrangements with intellectual deficiency and/or congenital malformations. *J Med Genet* **50**, 144–150, doi:10.1136/jmedgenet-2012-101351 (2013).
- 11 Zhang, Q. *et al.* Impaired Dendritic Development and Memory in Sorbs2 Knock–Out Mice. *J Neurosci* **36**, 2247–2260, doi:10.1523/JNEUROSCI.2528-15.2016 (2016).
- 12 Lee, S. E. *et al.* nArgBP2 regulates excitatory synapse formation by controlling dendritic spine morphology. *Proc Natl Acad Sci U S A* **113**, 6749–6754, doi:10.1073/pnas.1600944113 (2016).
- 13 Zhao, H. & Nyholt, D. R. Gene–based analyses reveal novel genetic overlap and allelic heterogeneity across five major psychiatric disorders. *Hum Genet* **136**, 263–274, doi:10.1007/s00439-016-1755-6 (2017).
- 14 Han, K. *et al.* SHANK3 overexpression causes manic–like behaviour with unique pharmacogenetic properties. *Nature* **503**, 72–77, doi:10.1038/nature12630 (2013).
- 15 Lee, S. E., Kim, J. A. & Chang, S. nArgBP2–SAPAP–SHANK, the core postsynaptic triad associated with psychiatric disorders. *Exp Mol Med* **50**, 1–9, doi:10.1038/s12276-017-0018-5 (2018).
- 16 Alberti, S. & Dormann, D. Liquid–Liquid Phase Separation in Disease. *Annu Rev Genet* **53**, 171–194, doi:10.1146/annurev-genet-112618-043527 (2019).
- 17 Banani, S. F., Lee, H. O., Hyman, A. A. & Rosen, M. K. Biomolecular condensates: organizers of cellular biochemistry. *Nat Rev Mol Cell Biol* **18**, 285–298, doi:10.1038/nrm.2017.7 (2017).
- 18 Li, P. *et al.* Phase transitions in the assembly of multivalent signalling proteins. *Nature* **483**, 336–340, doi:10.1038/nature10879 (2012).
- 19 Shin, Y. *et al.* Spatiotemporal Control of Intracellular Phase Transitions Using Light–Activated optoDroplets. *Cell* **168**, 159–171 e114, doi:10.1016/j.cell.2016.11.054 (2017).
- 20 Zhao, H. *et al.* SCAMP5 plays a critical role in synaptic

- vesicle endocytosis during high neuronal activity. *J Neurosci* **34**, 10085–10095, doi:10.1523/JNEUROSCI.2156–14.2014 (2014).
- 21 Rodriguez, A., Ehlenberger, D. B., Dickstein, D. L., Hof, P. R. & Wearne, S. L. Automated three–dimensional detection and shape classification of dendritic spines from fluorescence microscopy images. *PLoS One* **3**, e1997, doi:10.1371/journal.pone.0001997 (2008).
- 22 Choi, J. *et al.* DXplorer: A Unified Visualization Framework for Interactive Dendritic Spine Analysis using 3D Morphological Features. *IEEE Trans Vis Comput Graph* **PP**, doi:10.1109/TVCG.2021.3116656 (2021).
- 23 Lu, W. *et al.* Activation of synaptic NMDA receptors induces membrane insertion of new AMPA receptors and LTP in cultured hippocampal neurons. *Neuron* **29**, 243–254, doi:10.1016/s0896–6273(01)00194–5 (2001).
- 24 Fortin, D. A. *et al.* Long–term potentiation–dependent spine enlargement requires synaptic Ca²⁺–permeable AMPA receptors recruited by CaM–kinase I. *J Neurosci* **30**, 11565–11575, doi:10.1523/JNEUROSCI.1746–10.2010 (2010).
- 25 Lisman, J., Yasuda, R. & Raghavachari, S. Mechanisms of CaMKII action in long–term potentiation. *Nat Rev Neurosci* **13**, 169–182, doi:10.1038/nrn3192 (2012).
- 26 Moriguchi, S., Shioda, N., Han, F., Narahashi, T. & Fukunaga, K. CaM kinase II and protein kinase C activations mediate enhancement of long–term potentiation by nefiracetam in the rat hippocampal CA1 region. *J Neurochem* **106**, 1092–1103, doi:10.1111/j.1471–4159.2008.05440.x (2008).
- 27 Wang, C. *et al.* GPS 5.0: An Update on the Prediction of Kinase–specific Phosphorylation Sites in Proteins. *Genomics Proteomics Bioinformatics* **18**, 72–80, doi:10.1016/j.gpb.2020.01.001 (2020).
- 28 Park, D. *et al.* Cooperative function of synaptophysin and synapsin in the generation of synaptic vesicle–like clusters in non–neuronal cells. *Nat Commun* **12**, 263, doi:10.1038/s41467–020–20462–z (2021).
- 29 Wu, X. *et al.* RIM and RIM–BP Form Presynaptic Active–Zone–like Condensates via Phase Separation. *Mol Cell* **73**,

- 971–984 e975, doi:10.1016/j.molcel.2018.12.007 (2019).
- 30 Kato, M. & McKnight, S. L. A Solid–State Conceptualization of Information Transfer from Gene to Message to Protein. *Annu Rev Biochem* **87**, 351–390, doi:10.1146/annurev-biochem-061516-044700 (2018).
- 31 Lin, Y. *et al.* Toxic PR Poly–Dipeptides Encoded by the C9orf72 Repeat Expansion Target LC Domain Polymers. *Cell* **167**, 789–802 e712, doi:10.1016/j.cell.2016.10.003 (2016).
- 32 Hayashi, Y., Ford, L. K., Fioriti, L., McGurk, L. & Zhang, M. Liquid–Liquid Phase Separation in Physiology and Pathophysiology of the Nervous System. *J Neurosci* **41**, 834–844, doi:10.1523/JNEUROSCI.1656-20.2020 (2021).
- 33 Strzyz, P. Phase separation tunes signal transduction. *Nat Rev Mol Cell Biol* **20**, 263, doi:10.1038/s41580-019-0121-7 (2019).
- 34 Brangwynne, C. P. *et al.* Germline P granules are liquid droplets that localize by controlled dissolution/condensation. *Science* **324**, 1729–1732, doi:10.1126/science.1172046 (2009).
- 35 Hosokawa, T. *et al.* CaMKII activation persistently segregates postsynaptic proteins via liquid phase separation. *Nat Neurosci* **24**, 777–785, doi:10.1038/s41593-021-00843-3 (2021).
- 36 Bugaj, L. J., Choksi, A. T., Mesuda, C. K., Kane, R. S. & Schaffer, D. V. Optogenetic protein clustering and signaling activation in mammalian cells. *Nat Methods* **10**, 249–252, doi:10.1038/nmeth.2360 (2013).
- 37 Roignot, J., Bonacci, T., Ghigo, E., Iovanna, J. L. & Soubeyran, P. Oligomerization and phosphorylation dependent regulation of ArgBP2 adaptive capabilities and associated functions. *PLoS One* **9**, e87130, doi:10.1371/journal.pone.0087130 (2014).
- 38 Kim, Y. *et al.* Phosphorylation of WAVE1 regulates actin polymerization and dendritic spine morphology. *Nature* **442**, 814–817, doi:10.1038/nature04976 (2006).
- 39 Soderling, S. H. *et al.* A WAVE–1 and WRP signaling complex regulates spine density, synaptic plasticity, and memory. *J Neurosci* **27**, 355–365,

- doi:10.1523/JNEUROSCI.3209-06.2006 (2007).
- 40 Khatau, S. B. *et al.* A perinuclear actin cap regulates nuclear shape. *Proc Natl Acad Sci U S A* **106**, 19017–19022, doi:10.1073/pnas.0908686106 (2009).
- 41 Milovanovic, D., Wu, Y., Bian, X. & De Camilli, P. A liquid phase of synapsin and lipid vesicles. *Science* **361**, 604–607, doi:10.1126/science.aat5671 (2018).
- 42 Zeng, M. *et al.* Reconstituted Postsynaptic Density as a Molecular Platform for Understanding Synapse Formation and Plasticity. *Cell* **174**, 1172–1187 e1116, doi:10.1016/j.cell.2018.06.047 (2018).
- 43 Chen, X., Wu, X., Wu, H. & Zhang, M. Phase separation at the synapse. *Nat Neurosci* **23**, 301–310, doi:10.1038/s41593-019-0579-9 (2020).
- 44 Araki, Y., Zeng, M., Zhang, M. & Huganir, R. L. Rapid dispersion of SynGAP from synaptic spines triggers AMPA receptor insertion and spine enlargement during LTP. *Neuron* **85**, 173–189, doi:10.1016/j.neuron.2014.12.023 (2015).
- 45 Boeynaems, S. *et al.* Phase Separation of C9orf72 Dipeptide Repeats Perturbs Stress Granule Dynamics. *Mol Cell* **65**, 1044–1055 e1045, doi:10.1016/j.molcel.2017.02.013 (2017).
- 46 El Fatimy, R. *et al.* Tracking the Fragile X Mental Retardation Protein in a Highly Ordered Neuronal RiboNucleoParticles Population: A Link between Stalled Polyribosomes and RNA Granules. *PLoS Genet* **12**, e1006192, doi:10.1371/journal.pgen.1006192 (2016).
- 47 Vernon, R. M. *et al.* Pi–Pi contacts are an overlooked protein feature relevant to phase separation. *Elife* **7**, doi:10.7554/eLife.31486 (2018).
- 48 Rosahl, T. W. *et al.* Essential functions of synapsins I and II in synaptic vesicle regulation. *Nature* **375**, 488–493, doi:10.1038/375488a0 (1995).
- 49 Koronakis, V. *et al.* WAVE regulatory complex activation by cooperating GTPases Arf and Rac1. *Proc Natl Acad Sci U S A* **108**, 14449–14454, doi:10.1073/pnas.1107666108 (2011).
- 50 Walikonis, R. S. *et al.* Densin-180 forms a ternary complex with the (alpha)-subunit of Ca²⁺/calmodulin-dependent protein kinase II and (alpha)-actinin. *J Neurosci* **21**, 423–

- 433 (2001).
- 51 Tao-Cheng, J. H. *et al.* Sustained elevation of calcium induces Ca(2+)/calmodulin-dependent protein kinase II clusters in hippocampal neurons. *Neuroscience* **106**, 69–78, doi:10.1016/s0306-4522(01)00262-7 (2001).
- 52 Nicole, O. & Pacary, E. CaMKIIbeta in Neuronal Development and Plasticity: An Emerging Candidate in Brain Diseases. *Int J Mol Sci* **21**, doi:10.3390/ijms21197272 (2020).
- 53 Bayer, K. U., Lohler, J., Schulman, H. & Harbers, K. Developmental expression of the CaM kinase II isoforms: ubiquitous gamma- and delta-CaM kinase II are the early isoforms and most abundant in the developing nervous system. *Brain Res Mol Brain Res* **70**, 147–154, doi:10.1016/s0169-328x(99)00131-x (1999).
- 54 Nicole, O. *et al.* A novel role for CAMKIIbeta in the regulation of cortical neuron migration: implications for neurodevelopmental disorders. *Mol Psychiatry* **23**, 2209–2226, doi:10.1038/s41380-018-0046-0 (2018).
- 55 Vyleta, N. P. & Snyder, J. S. Prolonged development of long-term potentiation at lateral entorhinal cortex synapses onto adult-born neurons. *PLoS One* **16**, e0253642, doi:10.1371/journal.pone.0253642 (2021).
- 56 Collitti-Klausnitzer, J., Hagen, H., Dubovyk, V. & Manahan-Vaughan, D. Preferential frequency-dependent induction of synaptic depression by the lateral perforant path and of synaptic potentiation by the medial perforant path inputs to the dentate gyrus. *Hippocampus* **31**, 957–981, doi:10.1002/hipo.23338 (2021).
- 57 Kim, E. *et al.* GKAP, a novel synaptic protein that interacts with the guanylate kinase-like domain of the PSD-95/SAP90 family of channel clustering molecules. *J Cell Biol* **136**, 669–678, doi:10.1083/jcb.136.3.669 (1997).
- 58 Kornau, H. C., Schenker, L. T., Kennedy, M. B. & Seeburg, P. H. Domain interaction between NMDA receptor subunits and the postsynaptic density protein PSD-95. *Science* **269**, 1737–1740, doi:10.1126/science.7569905 (1995).
- 59 Naisbitt, S. *et al.* Shank, a novel family of postsynaptic density proteins that binds to the NMDA receptor/PSD-

- 95/GKAP complex and cortactin. *Neuron* **23**, 569–582, doi:10.1016/s0896-6273(00)80809-0 (1999).
- 60 Xiao, B. *et al.* Homer regulates the association of group 1 metabotropic glutamate receptors with multivalent complexes of homer-related, synaptic proteins. *Neuron* **21**, 707–716, doi:10.1016/s0896-6273(00)80588-7 (1998).
- 61 Amerio, A., Odone, A., Liapis, C. C. & Ghaemi, S. N. Diagnostic validity of comorbid bipolar disorder and obsessive-compulsive disorder: a systematic review. *Acta Psychiatr Scand* **129**, 343–358, doi:10.1111/acps.12250 (2014).
- 62 Chen, Y. W. & Dilsaver, S. C. Comorbidity for obsessive-compulsive disorder in bipolar and unipolar disorders. *Psychiatry Res* **59**, 57–64, doi:10.1016/0165-1781(95)02752-1 (1995).
- 63 Raja, M. & Azzoni, A. Comorbidity of Asperger's syndrome and Bipolar disorder. *Clin Pract Epidemiol Ment Health* **4**, 26, doi:10.1186/1745-0179-4-26 (2008).
- 64 Xie, J. *et al.* Positive and negative relationship between anxiety and depression of patients in pain: a bifactor model analysis. *PLoS One* **7**, e47577, doi:10.1371/journal.pone.0047577 (2012).
- 65 Schork, A. J. *et al.* A genome-wide association study of shared risk across psychiatric disorders implicates gene regulation during fetal neurodevelopment. *Nat Neurosci* **22**, 353–361, doi:10.1038/s41593-018-0320-0 (2019).
- 66 Wu, Y. *et al.* Multi-trait analysis for genome-wide association study of five psychiatric disorders. *Transl Psychiatry* **10**, 209, doi:10.1038/s41398-020-00902-6 (2020).
- 67 Gandal, M. J. *et al.* Shared molecular neuropathology across major psychiatric disorders parallels polygenic overlap. *Science* **359**, 693–697, doi:10.1126/science.aad6469 (2018).
- 68 Lee, S. E., Kim, J. A. & Chang, S. nArgBP2-SAPAP-SHANK, the core postsynaptic triad associated with psychiatric disorders. *Exp Mol Med* **50**, 2, doi:10.1038/s12276-017-0018-5 (2018).
- 69 Shih, P. Y. *et al.* Phase separation and zinc-induced

transition modulate synaptic distribution and association of autism-linked CTTNBP2 and SHANK3. *Nat Commun* **13**, 2664, doi:10.1038/s41467-022-30353-0 (2022).

- 70 tom Dieck, S. *et al.* Bassoon, a novel zinc-finger CAG/glutamine-repeat protein selectively localized at the active zone of presynaptic nerve terminals. *J Cell Biol* **142**, 499–509, doi:10.1083/jcb.142.2.499 (1998).
- 71 Fenster, S. D. *et al.* Piccolo, a presynaptic zinc finger protein structurally related to bassoon. *Neuron* **25**, 203–214, doi:10.1016/s0896-6273(00)80883-1 (2000).

국문초록

액상 간 상분리 현상을 통한
nArgBP2의
구조적 가소성 조절 기전에 관한 연구

서울대학교 대학원

의과학과

조 은 지

수상돌기가시는 뇌에서 대부분의 흥분성 시냅스 신호를 받는 수상돌기의 구조이며 주로 액틴 필라멘트로 이루어져 있다. 수상돌기가시의 형태는 매우 다양하며 수많은 액틴 조절 단백질들에 의해 역동적으로 조절된다. nArgBP2는 흥분성 시냅스의 형성과 기능에 중요한 단백질로 알려져 있으며 nArgBP2의 유전적 결실은 인간의 지적장애와 유사한 행동을 쥐에서 유발한다는 연구결과도 있다. 이전의 연구결과에서는 발달 단계의 신경세포에서는 RNA 간섭에 의한 nArgBP2 발현 저해가 수상돌기가시 형성에 영향을 주어 정상적인 형태의 수상돌기가시가 아닌 펠로포디아의 형성을 증가시켰다. 하지만 이미 수상돌기가시 형성이 완료된 후 신경세포에서 nArgBP2 발현 저해에서는 수상돌기가시의 형태에 아무런 영향을 끼치지 않았다. 발달단계의 신경세포와 같이 구조적 리모델링이 일어날 때 nArgBP2가 역할을 할 것이라고 추론하였고, 이를 확인

하기 위해 성숙한 신경세포에서 구조적 리모델링을 일으킬 수 있는 화학적 장기강화 (cLTP: chemical long-term potentiation)을 유도해보았다. 화학적 장기강화를 일으켰을 때 컨트롤 세포의 수상돌기가시는 그 크기가 커지는 반면 nArgBP2 발현이 저해된 신경세포에서는 크기가 변하지 않거나 작아지는 현상을 보였다. 이는 같은 조건에서 초고해상도 이미징을 통해 3차원 구조의 형태학적 측정값을 확인한 결과, 성숙한 신경세포에서는 nArgBP2의 결핍이 수상돌기가시의 머리 크기 확대를 저해함을 알 수 있었다.

성숙한 신경세포에서 화학적 장기강화가 유도되었을 때 nArgBP2의 형태를 라이브 이미징으로 관찰하고자 nArgBP2 발현 저해와 동시에 shRNA 저항 nArgBP2를 발현시켜 관찰하였다. 그 결과 대부분의 nArgBP2가 수상돌기가시에 응집체 형태로 존재하고, 화학적 장기강화가 유도되면 그 응집체가 분산되는 현상을 보였다. 또한, 응집체가 분산되면서 수상돌기가시의 머리 크기가 커지는 것이 관찰되었다. 이러한 현상은 nArgBP2의 SH3 도메인만 존재할 때도 확인할 수 있었다.

nArgBP2의 SH3 도메인에 칼슘/칼모듈린 인산화 부위로 추정되는 부분이 존재하며, 이 잔기들이 모두 보존되는 것을 보아 화학적 장기강화 동안 칼슘/칼모듈린 인산화에 의해 nArgBP2가 영향을 받을 것이라고 추론하였다. 이를 확인하고자 인산화 결핍 돌연변이를 만들어 동일하게 신경세포에서 라이브 이미징한 결과, 응집체가 분산되지 않으며 수상돌기가시의 머리 크기 또한 커지지 않는 것을 확인하였다. 이러한 결과는 화학적 장기강화 동안 nArgBP2 응집체의 확산 및 수상돌기 가시의 머리 크기 확대에는 칼슘/칼모듈린에 의한 인산화가 필요함을 나타낸다.

화학적 장기 강화 동안 nArgBP2 응집체의 확산을 보아 응집체가 고체와 같은 집합체가 아니라 액체-액체 상 분리에 의해 발생하는 액체와 같은 응집체와 유사하다고 추론하였고, 이를 확인하고자 액상 간 상 분리에 의한 응집체를 확산시킨다고 알려진 헥산다이올을 처리해서 응집체가 확산하는 것을 확인하였다. 또한, 신경세포뿐만 아니라 COS7 세포에서도 SH3 도메인으로 액상 간 상 분리를 통해 응집체를 이루고, 정제된

단백질에서도 액상 간 상 분리에 의한 응집체를 형성하는 것을 확인할 수 있었다. 앞서 신경세포에서 확인하였던 것처럼 COS7 세포에서 칼슘/칼모둘린에 의한 nArgBP2 응집체 확산을 관찰하였다

화학적 장기강화가 일어나는 동안 nArgBP2로 인한 수상돌기가시 확대는 WAVE1 상호 작용에 의해 조절된다. WAVE1은 Arp2/3 복합체를 통해 신호를 전달하여 액틴 중합을 조절하여 수상돌기가시를 확대하는 것으로 알려져 있으며, 우리는 이전에 nArgBP2가 WAVE를 통해 수상돌기가시 형태를 조절한다는 것을 밝혀내었다. 따라서 WAVE1과 nArgBP2 사이의 상호 작용이 화학적 장기강화 동안 수상돌기가시 확대에 필요하다는 추론을 하였다. 이 가설을 확인하고자 화학적 장기강화 자극 동안 WAVE1과 nArgBP2 간의 상호 작용을 차단하기 위해 nArgBP2에 미토콘드리아 표적 태그를 달아 세포질에서 미토콘드리아로 격리하였다. 그 결과 nArgBP2가 화학적 장기강화 동안 응축물에서 분산될 것으로 예상하지만 확산된 ArgBP2는 미토콘드리아로 격리되기 때문에 WAVE1과 상호작용할 수 없고 그로 인해 수상돌기가시가 커지지 않는 것을 확인하였다.

최근 시냅스 전후에는 액상 간 상 분리 어셈블리가 포함될 수 있다는 연구결과가 보고되었으며, 이는 뉴런 시냅스 내 및 사이의 신호 전달을 조절하는 데 중요하다고 밝혀지고 있다. SynGAP 및 FMRP(Fragile X Mental Retardation Protein)는 액상 간 상 분리를 일으키는 것으로 밝혀졌고, PSD95, GKAP 등 시냅스 후 단백질도 액상 간 상 분리를 통해 응축된 어셈블리를 생성한다는 연구결과도 있다. nArgBP2가 다른 시냅스 후 단백질과 응축물을 형성하는지와 nArgBP2 응축물의 형성이 다른 시냅스 단백질에 의해 영향을 받는지 향후 연구를 통해 밝혀낼 수 있을 것이다. 이러한 단백질의 활성화에 대한 액상 간 상 분리 조절은 증상이 겹치는 여러 신경 정신 장애의 기본 메커니즘을 이해하기 위한 새로운 기회를 제공할 수도 있을 것이다.

또한, nArgBP2에는 NSE라는 특이적인 도메인이 존재하며 도메인 내에는 zinc finger 모티프가 있다고 알려져 있다. 하지만 이러한 NSE의

역할은 아직 밝혀진 바가 없다. NSE의 역할을 알고자 NSE 도메인이 존재하지 않는 돌연변이를 발현시킨 결과, nArgBP2가 수상돌기가시에 덜 존재하는 것으로 보아 NSE 도메인이 nArgBP2의 정상적인 위치 발현에 중요함을 알 수 있었다. 또한 높은 농도의 아연을 처리했을 때에도 마찬가지로 nArgBP2의 발현위치가 달라지는 것을 확인하였다. 이를 통해 정상적인 뇌 기능에 중요하다고 알려진 아연과의 결합과 또 다른 시냅스 단백질과의 연관성에 대한 추가 연구가 필요함을 알 수 있었다.

본 내용은 Exp Mol Med 에 출판 완료된 내용임.

주요어: 액상 간 상분리, nArgBP2, 수상돌기가시, 구조적 가소성

학 번 : 2016-23695